Analysis and design of close operations at Phobos

David Belsa Prieto
Escuela Politécnica Superior (EPS)
Universidad Carlos III de Madrid

A thesis submitted for the degree of
Bachelor in Aerospace Engineering

Madrid, June 2016

A mis padres, por su apoyo incondicional durante toda mi vida, especialmente en estos cuatro años lejos de casa. Su sacrificio, su trabajo duro y la confianza depositada, aún a riesgo de que me pudiera quedar por el camino, han supuesto para mí la fuerza necesaria para poder plantearme ir a por todo, ya que los límites, como los miedos, son muchas veces simples imaginaciones.

También quiero dedicar unas líneas a todos aquellos antepasados míos que decidieron trabajar toda una vida para dar a sus descendientes la oportunidad de estudiar, leer y aprender; su incesante ritmo de trabajo y su sudor me han brindado las oportunidades que, lamentablemente, ellos nunca pudieron disfrutar.

Acknowledgements

First and foremost, I would like to thank Prof. Manuel Sanjurjo Rivo for the guidance and sage advice provided in this Thesis, which have contributed to not being stuck in the traps of the path; his commitment and patience have been invaluable in order to choose the working direction that had to be followed, making this Thesis a reality. His steadfast support provided an extra courage to make me work harder than ever, obtaining the results faster and expanding the contents that are presented in this document.

I would also like to acknowledge the availability and commitment of the PhD students David Morante González and Daniel González Arribas. David introduced me to the GPOPS program, being available at any time to solve doubts that could emerge when taking the first steps of the program. Daniel, on the other hand, has given us wise indications for creating alternative computational paths to overcome the computational resource difficulties found during these months.

Finally, as a concluding remark of this four-year degree, I have to say I am indebted to all the professors in the Aerospace department, who have been always opened to solve the doubts that have arisen when studying and doing laboratory sessions during the whole Aerospace Engineering degree, being comprehensive and committed for fixing in a perfect way the concepts learned.

Abstract

This Thesis presents the analysis of a descent maneuver to the Martian moon Phobos, treated mathematically as a Low-Thrust Optimal Control Problem. In order to increase the accuracy of the problem, the gravity acceleration at each of the trajectory nodes is obtained by applying the Polyhedron method, discussed in Chapter 2.

The following document is structured by discussing first the general aspects of the problem analyzed, focusing then completely on the Optimal Control Problem solved.

Firstly, the scientific aims that a mission to Phobos presents are discussed, together with the uncertainties that are still present when studying a mission to this Martian moon. Then, a theoretical approach to the Polyhedron method is discussed, as well as the reasons by which this method is chosen ahead of others.

From that point on, a closer approach to the problem is made; first, by making a general theoretical discussion about the numerical methods present in the GPOPS program that could be used to solve the problem stated, reasoning then the election made and the aspects that have prevailed for this decision to be taken. Subsequently, a detailed characterization of both the dynamical and path constraints implemented is made, as well as a brief description of the propulsive parameters chosen and the reference frame selected, in the same fashion as other articles [1] that treat a descent maneuver too.

Finally, the analysis is centered exclusively on the solving process followed. The computational work carried out is explained first, detailing the modifications made in order to overcome the computational resources' problem that arose. The results for the optimization are then presented, making a thorough description of the physical phenomena occurring in the spacecraft dynamics.

As concluding remarks, a summary of the results obtained is made, together with their limitations; a roadmap for future work is added too, setting the steps that should be taken in the future for making an even more realistic study, which could be used as a first pragmatic approach to propose a real mission to Phobos.

Contents

List of Figures

Chapter 1

Introduction

Phobos is the larger and innermost of the two Martian moons, with the outer one being Deimos. According to [5], Phobos is one of the deep-space human exploration activities proposed in order to enhance our knowledge of the Solar system and assess its validity as a bridge of future in-space transportation missions. It is a low-gravity object inside the Martian gravitational field, with low density and low albedo, and spectrally similar to D-type bodies present in the outer asteroid belt [6].

Phobos, as well as Deimos, are tidally synchronized to Mars, implying that they take as long to rotate around its own axis as they do to revolve around Mars; hence, the same side of Phobos is observed from this planet at all times. Phobos does have a nearly circular orbit, within a few degrees of the equatorial plane. The orbit altitude is another fundamental aspect to be considered, as it influences both the communications to Mars and the sunlight exposure [7].

Another aspect of interest is the amount of sunlight exposure that each region in Phobos' surface has, as well as its line of sight. According to [7], small regions near the crater Flimnap have complete line-of-sight to the full Mars' disk and continuous sunlight. Moreover, because of the closeness between Phobos and Mars, part of the Martian disk can be visible from the polar regions in the far side of Phobos. This phenomena can be observed in the following figure

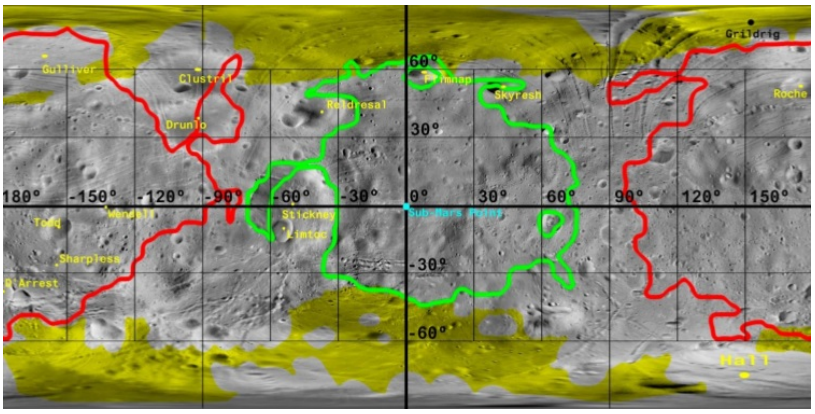

Figure 1.1: 2D Phobos surface. Yellow for regions of continuous sunlight. Green for regions with full line-of-sight to Mars. Regions between green and red have partial line of sight. Both northern summer and southern summer seasons are represented; the north region has sunlight during the northern summer season, either continuous or discontinuous depending on the specific region analyzed; same reasoning for the south region.

As observed from Figure 1.1, there is an almost complete line of sight to Mars from regions with coordinates $40 - 45^0$S, having continuous sunlight too. Although these characteristics may make them potential destinations for a scientific mission to Phobos, a trade-off analysis must be made, since other aspects such as the radiation exposure and the magnetization forces have to enter into the study too.

These factors must be thoroughly analyzed before completing a descent maneuver to the Phobos surface, since they should enter as perturbations in the dynamical constraints of the problem. It must be noted, nonetheless, that these perturbations will not be included into the Low-Thrust Optimal Control problem studied, since a more detailed characterization of the Phobos magnetic phenomena [8] is required to be known beforehand. As explained in Chapter 5, future improvements of this problem should require to implement these perturbations, as well as the others specified in Section 5.2.

1.1 Motivation

Phobos (and Deimos) can constitute a scientific base to provide support for missions centered on Mars, as well as a platform for rapid-tempo telepresence activities on the Martian surface [5]. Both moons do not have a clear origin, with two main hypothesis prevailing nowadays:

- **They are outer solar system objects captured by the Martian gravity field [9].**

  This hypothesis would explain the low densities and albedos of both moons, as well as their spectral similarity to D-type asteroids; however, their circular and near-equatorial orbits with their tidal synchronization with Mars do not fit into this model, since these aspects are not compatible with the fact that both moons should have been captured in very specific conditions, as a consequence of the aerodynamic drag provoked by the young Mars' atmosphere (known as protoatmosphere) [10].

  This hypothesis would have, nonetheless, scientific interest too since, if Phobos is a captured asteroid, its chemical history could be analyzed and compared with data obtained from the meteorites studied, thus offering information about the materials present in the early stages of the Solar system.

- **They are In situ formed from Mars material [11].**

  This hypothesis avoids explaining the capture of both moons; in fact, asserting its validity would imply that the materials they are composed of are similar to those of bulk Mars. Hence, the composition at the pre-Noachian period could be analyzed.

  Note that an analysis on Mars' surface would imply fracturing the pre-Noachian crust in order to obtain samples from it, since the materials that composed the Martian surface formed at the early stages of Mars are at a considerable distance from the actual surface; consequently, they would be much less reliable for the study than those obtained directly from the surfaces of Phobos or Deimos, which could be even encountered as regolith [6].

In order to summarize both hypothesis, the following table is provided.

Origin Hypothesis	Composition predicted	Elemental abundances	Mineral abundances
Capture of organic and water-rich outer solar system body.	Ultra-primitive composition.	High C; high Zn/Mn; high S	Abundant phyllosilicates; carbonates and organic phases; anhydrous silicate phases rare.
Capture of organic- and water-poor outer solar system body.	Anhydrous silicates plus elemental carbon.	High C; Mg/Fe ratio ∼2-4;	Anhydrous, med. Fe(20-40%) pyroxene + olivine; abundant amorphous carbon or graphite?
Capture of inner solar system body.	Composition like common meteorites.	Mg/Si ∼ 0.8-1, Al/Si ∼ 0.05-0-1, Zn/Mn & Al/Mn ratios; low C expected.	Low carbonates, phyllosilicates; pyroxene, olivine probably in range of known meteorites.
Co-accretion with Mars.	Bulk Mars; similar to ordinary chondrites but specific SNC-derived comp.	Mg/Si, Al/Si, Fe/Si indicative of bulk Mars; low C; Zn/Mn, Al/Mn like ordinary chondrites.	Anhydrous silicates with Fe, Mg of bulk Mars; low abundance of C-bearing phases.
Giant impact on Mars.	Evolved martian crust or mantle.	High Al/Si, Ca/Si, lower Fe/Si, Mg/Si indicative of evolved igneous materials.	Evolved, basaltic mineralogy consistent with datasets for Mars.

Table 1.1: Compositions predicted for each of the Phobos origin hypothesis (from [12]).

Apart from the previously mentioned facts, there are also strategic gaps of knowledge of great scientific importance [12]

- Whether there is hydroxyl or hydrogen in bound water. The amount of OH is not known, and may be present at Phobos surface just due to the solar wind; being intrinsic to it is another option that is not discarded.[6]
- Whether carbon is available.
- The potential radiation hazards close to Phobos.
- The logistics of space operation at Phobos, as the conditions at Phobos' surface could make technology feasible for an eventual mission to Mars.
- The chemical composition of regolith from Phobos' surface, which would give a greater insight into the Phobos origin.

The previously described gaps of knowledge are summarized in the next table

Knowledge gap	**Science/engineering objective**	**Measurement requirement**
What is the potential for in situ resource utilization from Phobos for a human mission to the Mars system.	Assess the potential for providing water and hydrogen and oxygen for fuel. Inventory the carbon resources for fuel production.	Determine abundances and characteristics of H_2O, OH-bearing phases. Measure abundances of organic, C-bearing phases.
What are the hazards for future astronauts in Mars orbit?	Determine human tissue effects of the radiation environment. Constrain the Mars orbital debris environment.	Measure radiation dose at different energy levels. Measure particle density of dust belts while in elliptical orbit before Phobos proximity operations.
What are the physical constraints on space operations near Phobos?	Determine global shape and rotational state. Determine the gravitational field with high fidelity.	Measure global shape using stereo imaging or laser altimetry. Measure mass and mass distribution using Doppler tracking during proximity operations.
What are the engineering issues associated with obtaining resources from Phobos?	Determine regolith composition.	Measure mineral and elemental abundances, particularly for hazardous phases.
	Measure regolith mechanical properties.	Determine geotechnical properties by imaging sample collection or with penetrometer.

Table 1.2: Gaps in knowledge required for human exploration of the Mars system (from [6]).

Finally, it must be remarked that *In Situ Resource Utilization* (ISRU) could make the mission more scientifically attractive (since more payload could be carried by the spacecraft), and cheaper, because the propellant could be obtained directly from Phobos [13], with carbon being combined with hydrogen in order to produce methane.

Besides, the most scientifically-interesting landing regions have been also studied, since they are a paramount aspect to be decided depending on the type of mission required; they can be appreciated in the following depiction

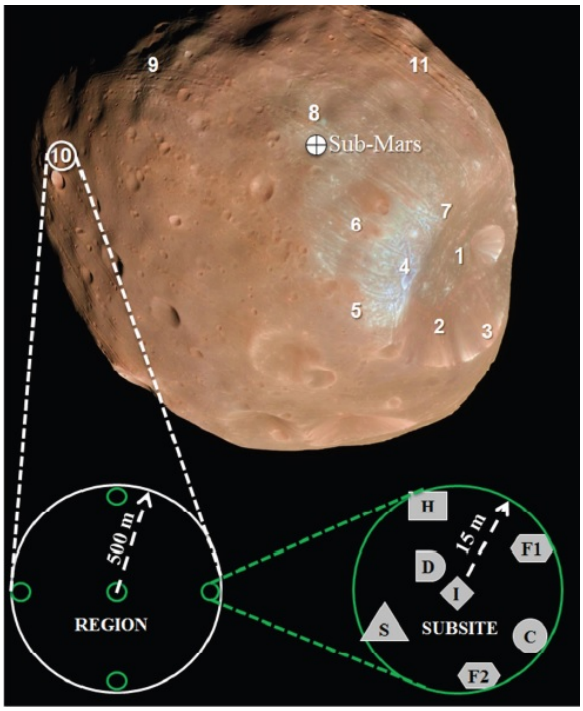

Figure 1.2: Regions of scientific interest on Phobos' surface (from [2]).

According to [2], the main important ones are

- Floor of Stickney Crater (1).
- Side wall of Stickney Crater (2).
- Far rim of Stickney Crater (3).
- Overturn of Stickney Crater and grooves (4).
- Young fresh crater (10)

Note that the enumeration corresponds to the zones marked in Figure 1.2, with only the most scientifically-interesting ones listed, following the author's criterion; in order to find the complete list, please refer to [2], in which a complete description of these important regions, among others of scientific interest is available.

Finally, there is another aspect that must be completely detailed before sending more probes to Phobos, i.e. whether Phobos possesses its own magnetosphere. The Phobos-2 spacecraft data should have solved this issue back in 1989, but it broke down before doing encounters with Phobos at 30-50 Km [14]; there was, nonetheless, magnetometric data obtained by this spacecraft at a near-Mars circular orbit, which is interpreted in four different ways [8]

- There is an interaction between the solar wind and the gas-dust torus at Phobos' orbit.
- There is a unusually distant bow shock and transition layer in the magnetosphere of Mars.
- There is a disturbance propagating with the solar wind.
- Phobos has its own magnetosphere, with the existence of its own dipole magnetic moment.

A new Phobos mission would completely determine which of the described hypothesis is valid, with future missions taking into account already this phenomenon. As aforementioned, the exact determination of Phobos' characteristics, origin and utilization as a scientific base for a Martian mission requires landing at its surface, the primary aspect covered in this Thesis. Because of the scientific interest that Phobos possesses, several studies have been made describing a future mission to this satellite; these studies have been focused, nonetheless, on describing different aspects from the Martian moon from a theoretical-qualitative approach, such as its composition or the magnetic phenomena occurring at or near its surface, studied in detail in [8], [15], [2] and [6]; however, none of them has been focused on studying quantitatively a descent maneuver on the surface of this satellite. Therefore, the main contribution that this analysis provides is a descent maneuver treated as a Low-Thrust Optimal Control Problem, with the Polyhedron method implemented in order to obtain a more accurate gravity computation (as compared to the case in which the body analyzed is assumed to be perfectly circular, with the gravity parameter taking an equal value for a given distance from the center of body, for any azimuthal and elevation angles combination). The gravity calculation is based on the development provided in [16], with some modifications made, as explained in Chapter 4. The landing maneuver, treated as a Low-Thrust Optimal Control Problem, is computed by using the program GPOPS, with the theoretical background developed in Chapter 2.

1.2 Thesis outline

The outline of this Thesis has been laid out as follows

- In **Chapter 2**, the theoretical background required is fully described. An introduction has been previously made, in which a general description of the problem

stated has been carried out. The election of the two methods requires a justification, i.e. which is the gravity model implemented, and which numerical method is chosen in order to solve the Non-Linear Programming (NLP) problem present in GPOPS, since many different options could be used. Hence, the chapter is divided into two different sections, namely:

  - The **Gravitational model** part, in which a description of the Polyhedron method is made, with an introductory discussion dealing with the facts that led to its selection ahead of other methods, such as the Spherical Harmonics gravitational model.
  - The **Optimal Control** part, in which the different numerical methods available to solve the Optimal Control Problem are briefly discussed, with a previous description also made accounting for the process by which the continuous Bolza Optimal Control Problem is transformed into a nonlinear programming problem (NLP) in the Pseudospectral case. At the end of the explanation, the numerical method used to obtain the results presented in this Thesis is stated, as well as the reasons that have led to such choice.

- In **Chapter 3**, a detailed description of the problem that is going to be solved is made. The dynamical model is established, as well as the propulsive characteristics and the type of departure orbits that can be followed. Finally, the Low-Thrust Optimal Control Problem is set, with its dynamical and path constraints.

- In **Chapter 4**, a presentation of the results is carried out. Firstly, the computational work made is outlined, explaining the implementation of the Low-Thrust Optimal Control Problem into GPOPS, together with its dynamical and path constraints. Next, the interpolation method used for computing the acceleration at each of the nodes is defined, together with a characterization of its associated error. As defined in this Chapter, the interpolation method had to be implemented in order to obtain an approximated value of the acceleration at each of the spacecraft trajectory nodes, since the lack of sufficient computer resources implied that the Polyhedron method to calculate the acceleration at each of the nodes could not be directly used. Then, the trajectory followed in order to perform the descent maneuver is stated and its limits defined. Finally, a discussion of the results is made, asserting that an optimal solution has been found for the Optimal Control Problem studied.

- In **Chapter 5**, the conclusions that can be extracted from the problem analyzed are highlighted, as well as the next steps required for decreasing the uncertainty in the dynamical constraints. The limitations in the results are also pointed out, in order to clearly state the boundaries present in the computations.

Chapter 2

Theoretical background

2.1 Introductory remarks

In this chapter, a description of the gravitational model used in the Low-Thrust Optimal Control Problem solved is made, together with an explanation of the GPOPS program used; a final section is also included, fully dedicated to the implementation of the problem studied into the GPOPS program. Once the gravitational model and the numerical methods to solve the Optimal Control Problem in GPOPS have been stated, the problem is thoroughly defined in Chapter 3.

The polyhedron method used for modeling the gravity acceleration is described first; an introductory discussion of the different gravitational models is presented right up front, continuing with a detailed explanation of the Polyhedron model, in which a summary of the analytical expressions that enter into the dynamic model is made. The implementation of this model is based on the work developed by [16]; some modifications have been made to the code, which are described in Chapter 4, together with all the computational work developed.

In the second part of this chapter, the Gauss Pseudospectral Method and the Collocation Method are presented, as they are the two numerical methods available to solve the Optimal Control Problem in GPOPS; in a similar fashion to the previous model described, a brief introductory discussion of the different methods available for solving the Optimal Control Problem is made with the aim of justifying the election done. Then, the analysis is centered on describing the transformation of the continuous Bolza problem into a Non-linear Programming Problem (NLP). Finally, the collocation Method is described, clearly stating its differences when compared to the Gauss Pseudospectral Method. After describing both methods, the one used in GPOPS to solve the Low-Thrust Optimal Control Problem is stated, with the corresponding explanation of the arguments that have led to such decision.

2.2 Gravitational Model

As previously stated, the spacecraft dynamics will account for the irregularities in Phobos' shape through the Polyhedron gravitational model of the Phobos gravity field. This model will give the exact acceleration value (within the validity of the hypothesis made) at each of the trajectory discretization points, known as nodes. This will, in turn, decrease the uncertainty of the Optimal Control Problem solution. Before getting to that point, however, the gravitational method must be described first; hence, in order to set the main concepts in a clear way, a summary at the end of the section is included, in which the main equations that enter into the Polyhedron code are highlighted.

The gravitational acceleration can be described by the following expression

$$\vec{g} = G \int_{Body} \frac{\rho\,(\vec{s})\;(\vec{r}-\vec{s})}{|\vec{r}-\vec{s}|}\,\mathrm{d}^3\vec{s}. \tag{2.1}$$

in which ρ accounts for the central body density, $\vec{r}$ is the field point and $\vec{s}$ is the distance to the field elements.

Note that, according to Newton, the gravity force produces a conservative force field; thus, the gravity vector field is the gradient of a scalar potential, referred to as U henceforth.

$$\nabla U = \vec{g} \tag{2.2}$$

The characterization of the gravitational field of a near-circular body can be made, in a first approximation, by considering it completely circular, thus implying that the value of the gravity parameter is constant for a given distance from the center of the body. Unfortunately, this approximation does not sustain by itself when dealing with irregularly-shaped objects. Because of that, other methods have been developed to accurately define the gravitational field of such bodies, and a complete explanation is included next to define each of them, and state their differences.

The study of gravitational fields for non-spherical bodies has its roots at the beginning of the twentieth century, with the first remarkable paperwork developed in the 1930s.

As aforementioned, irregularly-shaped bodies are not large enough for self-gravitation to shape them into spheres [17]; hence, other methods are required, which are classified into three main categories

- Harmonic expansion

- Mass concentrations
- Polyhedron

The first major field of study was the representation of gravitational fields by **harmonic expansions**. This method consists in expanding the gravitational potential into a harmonic series, computing then the series coefficients. According to [18], the series coefficients are then evaluated as integrals over the volume of the body.

This method has, nonetheless, various drawbacks:

- The truncation error appearing when truncating the series expansion grows when the gravity field is analyzed near the radius of convergence of the model.
- Divergence effects become remarkable when evaluating the gravity field inside the reference sphere of the body, which can be defined as the smallest sphere that being centered at the origin of the reference frame circumscribes all the points of the body [3].
- There is no possible way to know whether a field point is within the body.

The second method is the **Mascon approach**, developed by [19]. In this method, the body is assumed to be composed of point masses distributed on an evenly spaced grid. Although this method is simpler to be developed than the Harmonic expansion method, it has some disadvantages:

- It cannot be ascertained whether a field point is within the body.
- Although simpler than the harmonic expansion method, it is less accurate.
- There are significant computational errors when dealing with a large number of mascons.

Please refer to [3], [19], [20] for a more detailed explanation of these methods.

In this Thesis, the method used will consist in modeling the irregularly-shaped body as a constant-density polyhedron, following the so-called Polyhedron method developed by [3].

This method has a great stronghold, namely: that the polyhedron can have all kinds of irregularities (concavities, voids, holes), with no error increment in the gravity field modeling. Moreover, it takes some advantages with respect to the previously described methods, with the more important ones included next:

- The accuracy of the gravitational field just depends on the errors due to the asteroid shape determination and its level of discretization.
- There are no divergence effects.
- The evaluation of the Laplacian of the gravitational potential can ascertain whether a field point is inside the polyhedron or not. If it inside, the partial differential equation will adopt the form of a Poisson's equation; if the field point is outside, the Laplace equation vanishes.

In addition to the previously described advantages, this method also allows a geometric interpretation from the solid angle subtended by a polyhedron face when viewed from the field point, a concept which will turn essential as the analysis advances.

It goes without saying that the Polyhedron model does also have drawbacks, as a model is always a representation of a reality. The two assumptions done in this case are

- The analyzed body is a polyhedron.
- Its density is constant.

With all the previous remarks in mind, the analysis can be started. It will be focused on computing the scalar potential function, since from this, both the acceleration vector field and the Laplacian can be calculated.

The potential U can be defined, according to (2.2) as

$$U \equiv G \iiint_M \frac{1}{q}\, dm = G\sigma \iiint_V \frac{1}{q}\, dV \tag{2.3}$$

where the assumption of constant density has been applied. Please note that the notation followed is that of [16], in order to provide a direct link to the method explained and computationally implemented; hence, the vector defining the distance in (2.1) and (2.3) is the same ($\vec{r} \equiv \vec{q}$).

Next, the Gauss divergence theorem is applied, in order to discretize the analysis over a surface, and not over a volume. The theorem relates both concepts by asserting that the expansion or contraction of a vector field through a given volume V (a phenomenon represented by the divergence quantity) is equal to the flux of the vector field through a given surface of this volume. Therefore

$$U \equiv G\sigma \iiint_V \frac{1}{q}\, dV = \frac{1}{2} G\sigma \iiint_V div\, \vec{q}\, dV = \frac{1}{2} G\sigma \iint_S \vec{n} \cdot \vec{q}\, dS \tag{2.4}$$

In order to apply the Gauss-divergence theorem, three conditions need to be fulfilled

- The volume must be bounded and connected.
- The surface must be piecewise smooth and orientable.
- The vector field and its first derivative must exist and be continuous both in the volume and the surface.

A possible source of error in the discretizing process might arise when analyzing polyhedron faces (triangles) with too small angles, which cause numerical instabilities. In order to avoid this, Delaunay Triangulation is applied. It can be understood the following way: with a set of points P in a plane, a Delaunay Triangulation can be defined as any angle-optimization triangulation of P.

After having derived the general 2D region potential, the study will be constrained to the analysis of a polygon. Hence, the following expression for the potential is obtained

$$U \equiv \frac{1}{2} G\sigma \sum_f \iint_f \vec{n}_f \cdot \vec{q}\, dS = \frac{1}{2} G\sigma \sum_f \vec{n}_f \cdot \vec{q}_f \iint_f \frac{1}{q}\, dS \tag{2.5}$$

By introducing into the analysis a 2D coordinate system centered on the field point, the following relation can be obtained

$$\iint_{polygon} \frac{1}{q} dS = \sum_e \int_e \frac{1}{q} \left(\Delta x d\Delta y - \Delta y d\Delta x\right) - \vec{n}_f \cdot \vec{q}_f\, \omega_f \tag{2.6}$$

Taking into account the following figure,

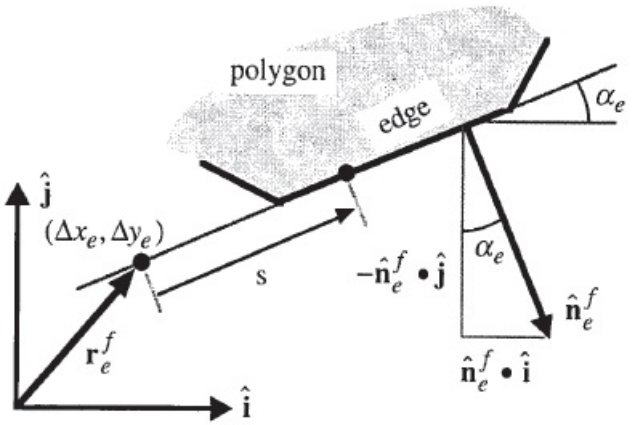

Figure 2.1: 2D representation of the distance from the field point to a general point along the edge. A typical edge "e" of polygon "f" is inclined by an angle α_e relative to the polygon's horizontal axis. The edge-normal vector $\vec{n_e}^f$ lies in the plane $\vec{i} - \vec{j}$, is perpendicular to the edge, and points outwards (from [3]).

a point can be expressed by the following relations

$$\Delta x = \Delta x_e + s\, cos\, \alpha_e \tag{2.7}$$

$$\Delta y = \Delta y_e + s\, sin\, \alpha_e \tag{2.8}$$

Therefore, the first term from expression (2.6) can be expressed as

$$\int_e \frac{1}{q} (\Delta x d\Delta y - \Delta y d\Delta x) = \vec{n}_e^f \cdot \vec{q}_e^f \int_e \frac{1}{q} ds \tag{2.9}$$

where the vector $\vec{q}_e^f$ can be expressed as

$$\vec{q}_e^f = \vec{i}\Delta x_e + \vec{j}\Delta y_e + \vec{k}\Delta z_e \tag{2.10}$$

The integral in expression (2.9) can be then written as

$$L_e^f = \int_e \frac{1}{q} ds = ln \frac{a+b+e}{a+b-e} \tag{2.11}$$

where a and b are the distances from the field point to each of the two ends of the edge, the vertices, while the parameter e accounts for the length of the edge. Then, by implementing expression (2.9) into (2.6), the following result arises

$$\iint_{polygon} \frac{1}{q} dS = \sum_e \vec{n}_e^f \cdot \vec{q}_e^f L_e^f - \vec{n}_f \cdot \vec{q}_f\, \omega_f \tag{2.12}$$

With this result, the potential from expression (2.5) can be expressed as

$$U = \frac{1}{2} G\sigma \sum_f \vec{n}_f \cdot \vec{q}_f \left(\sum_e \vec{n}_e^f \cdot \vec{q}_e^f \cdot L_e - \vec{n}_f \cdot \vec{q}_f \, \omega_f \right) \tag{2.13}$$

Please note that, according to the previous development, the computation of the potential would go twice through each of the edges as a consequence of the closed surface analysis. Therefore, the vector from the field point to a point in the edge (2.10) will be equal for each of the faces, while the parameter defined in (2.11) will be also the same; this is obvious, as the edge analyzed and its spacial position are the same, no matter the face analyzed. Hence, it is desirable to express the nested sum with only accounting for the edges and not the faces, in order not to perform the computation over each edge twice. The mathematical expression to this assertion takes the following form

$$\sum_f \left(\sum_e \vec{q}_e \cdot \vec{n}_f \vec{n}_e^f \cdot \vec{q}_e^f L_e^f \right) = \sum_e \vec{q}_e \cdot E_e \cdot \vec{q}_e \, L_e \tag{2.14}$$

where the parameter E_e represents a Dyad, which is defined as

$$E_{12} \equiv \vec{n}_A \vec{n}_{12}^A + \vec{n}_B \vec{n}_{21}^B \tag{2.15}$$

Please take the following figure as a reference in order to comprehend in a better way the previous expression (2.15)

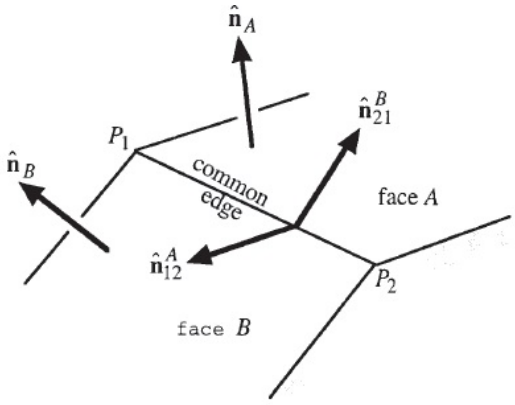

Figure 2.2: Normal and edge-normal from common-edge faces (from [3]).

Besides, a Dyad can be also defined for each face as follows

$$F_f \equiv \vec{n}_f \vec{n}_f \tag{2.16}$$

Both definitions of the Dyad are symmetric for all the coordinate systems, according to the development made by [3].

By introducing the previous expressions into (2.13), the potential of a polyhedron can be finally defined as

$$U = \frac{1}{2} G\sigma \sum_{e} \vec{q}_e \cdot E_e \cdot \vec{q}_e \, L_e - \frac{1}{2} G\sigma \sum_{f} \vec{q}_f \cdot F_f \cdot \vec{q}_f \, \omega_f \tag{2.17}$$

As pointed out by [16], the implementation of the Dyad has allowed the potential parameter to get free of nested sums, thus keeping the computational time increasing linearly with the number of polygons; with nested sums, the dependence was quadratic, thus consuming much more computational resources, especially in the Phobos case, for which the number of polygons required to define its shape is much greater than for an asteroid (Castalia, for instance).

Note that the implemented code must also evaluate whether an edge has been already stored or not, i.e. whether the same edge has been analyzed having entered as an edge of the contiguous surface. From [16], the function created to fulfill this task, "Link_Check", requires a humongous amount of memory, which in the Phobos case went up to 40 GB. Since no computational resources of such capacity were available, the previous function had to be modified, as explained in Chapter 4.

Next, keeping in mind that the potential is in fact a scalar, the attraction force that Phobos exerts on the spacecraft can be obtained by differentiating (2.17). The procedure can be fully observed in [3], in which a differentiation of the potential of a 2D polygon is made first, by applying Green's theorem. Then, the analysis is restricted for the planar region to be a polygon. Finally, by considering Phobos as a constant-density body, the following expression results

$$\vec{a} = G\sigma \sum_{e} E_e \cdot \vec{q}_e \cdot L_e + G\sigma \sum_{f} F_f \cdot \vec{q}_f \, \omega_f \tag{2.18}$$

When doing the computational analysis, the Laplacian needs to be introduced, in order to ascertain whether a field point is either outside or inside the polyhedron.

$$\nabla^2 U = -G\sigma \sum_{f} \omega_f \tag{2.19}$$

If the field point is outside the polyhedron, the parameter $\sum_f \omega_f$ in expression (2.19) will vanish; if it is inside, it will take a value equal to 4π.

As a final remark, it must be noted that the parameter ω_f included in expression (2.19) is defined as

$$\omega_f \equiv \iint_S \frac{\Delta z}{r^3} dS \tag{2.20}$$

and it can be interpreted as the signed area of S when projected onto a unit sphere centered on the field point.

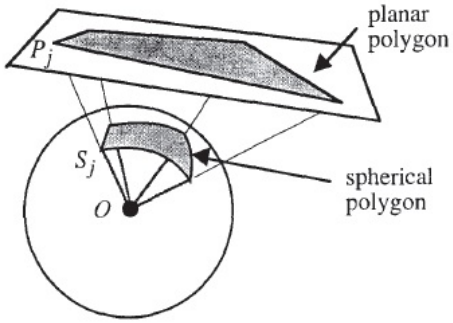

Figure 2.3: Spherical polygon created from the projection of a planar polygon onto a sphere (from [3]).

When the planar region of S is a polygon, the signed area is a spherical polygon with great-circular arcs as edges. Hence, the area of a spherical polygon in a sphere can be defined as

$$|\omega_f| = R^2 \left[\sum_{j=1}^{n} S_j - (n-2)\,\pi \right] = \sum_{j=1}^{n} S_j - (n-2)\,\pi \tag{2.21}$$

Note that a unit sphere is being considered in the analysis ($R = 1$). In expression (2.21), the parameter n refers to the number of vertices, while S_j accounts for the spherical vertex angles.

As stated by [16], the signed solid angle is the parameter consuming more computational time, since it takes 21 products, 20 additions, 1 division and 1 arctangent per face.

2.2.1 Summary

In the previous explanation, an exhaustive study of the Polyhedron method has been made, in order to clearly state in a theoretical way how the gravity code implemented operates. As a final summary, the three main expressions obtained from the previous study are embodied again, in order to highlight the main equations that result from the Polyhedron method analysis.

The **potential of a polyhedron** is defined as

$$U = \frac{1}{2} G\sigma \sum_{e} \vec{q}_e \cdot E_e \cdot \vec{q}_e L_e - \frac{1}{2} G\sigma \sum_{f} \vec{q}_f \cdot F_f \cdot \vec{q}_f \, \omega_f \tag{2.22}$$

The **acceleration vector field** is expressed by

$$\vec{a} = G\sigma \sum_{e} E_e \cdot \vec{q}_e \cdot L_e + G\sigma \sum_{f} F_f \cdot \vec{q}_f \, \omega_f \tag{2.23}$$

Finally, in order to assess whether a point is either inside or outside the body, **Laplace equation** is applied

$$\nabla^2 U = -G\sigma \sum_{f} \omega_f \tag{2.24}$$

2.3 Pseudospectral Method

The Optimization Problem is required to be defined as well, since the descent maneuver to Phobos' surface is going to be mathematically characterized by a Low-Thrust Optimal Control Problem. As stated in the analysis made by [21] and [22], the Optimization Control Problem is based on the optimization of the following performance index

$$J = \Phi \left[x(t_0), t_0, x(t_f), t_f; p \right] + \int_{t_0}^{t_f} L \left[x(t), u(t), t; p \right] dt \tag{2.25}$$

where $x(t)$ refers to the trajectory, $u(t)$ to the control, p to the static parameter, t_0 to the initial time, and t_f to the terminal time.

The continuous Bolza problem can be posed in a formal way as follows:

"*Determine the state/trajectory, $x(t) \in X \subset \mathbb{R}^{n_x}$, the control $u(t) \in U \subset \mathbb{R}^{n_u}$, the vector of static parameters* $\mathrm{p} \in P \subset \mathbb{R}^{n_p}$*, the initial time $t_0 \in \mathbb{R}$, and the terminal time $t_f \in \mathbb{R}$ that optimizes the expression defined in (2.25).*"

The dynamics of the system analyzed are defined by a set of differential equations, referred to as dynamic constraints

$$\dot{x}(t) = f \left[x(t), u(t), t; p \right] \tag{2.26}$$

subject to the initial t_0 and terminal t_f conditions

$$\phi_l \leq \phi \left[x(t_0), t_0, x(t_f), t_f, ; \mathrm{p} \right] \leq \phi_u \tag{2.27}$$

Moreover, the optimized solution must fulfill the path constraints imposed

$$g_l \leq g\left[x(t), u(t), t; \mathrm{p}\right] \leq g_u \tag{2.28}$$

Note that, when the objective function is expressed as in (2.25), it is referred to as the *Bolza form*. When it is composed of just the integral part, it is called *Lagrange form* and, when the integral is not present, it is referred to as the *Majer form*.

There are three different possible approaches in order to solve the Optimization problem [23]

- **Direct methods**.

  Direct methods have a larger radius of convergence; when direct shooting methods are used, the problem can be described with a small set of parameters. They are, however, less accurate than indirect methods.

- **Indirect methods**.

  Indirect methods produce the most accurate solutions when converging. They are, nonetheless, highly dependent on the boundary conditions; moreover, they require the optimality conditions to be derived analytically.

- **Pseudospectral methods**.

  Pseudospectral methods are used to obtain an accurate solution with few discretizations. When the problem's solution is smooth, they converge exponentially. Moreover, costate estimation procedures can be used to verify the optimality of the solution.

In this Thesis, the Pseudospectral method was one of the methods that were evaluated in order to solve the Optimal Control Problem, being the other the Collocation method. Both of them can be implemented in GPOPS, a general-purpose MATLAB software for solving continuous Optimal Control Problems, which implements global collocation using the Gauss pseudospectral method [24] and segment collocation by using the Collocation method (in case this method is properly coded into the GPOPS), as explained in detail in [25].

One of the main aspects in which Pseudospectral methods are based is the election of the interval of nodes (collocation points). In order to provide an insight, the three main important sets are briefly described

- **Legendre-Gauss (LG) points**. They lie on the open interval $\tau \in (-1, 1)$.

- **Legendre-Gauss-Radau (LGR)** points. They lie on the half open interval $\tau \in [-1, 1)$.
- **Legendre-Gauss-Lobatto (LGL) points**. They lie on the half open interval $\tau \in (-1, 1]$.

As the GPOPS program does operate on the basis of LG collocation points, these will be the ones used. Note that the Legendre-Gauss (LG) points are just the roots of the Nth-degree Legendre polynomial, denoted as $P_N(\tau)$. Please refer to [25] in order to find a more accurate description of the Legendre polynomials.

2.3.1 Gauss Pseudospectral Discretization

The Gauss Pseudospectral method is based on approximating both the state and control using interpolating polynomials.

- **State**. It is approximated by using N+1 Lagrange interpolating polynomials

$$x(\tau) \approx X(\tau) = \sum_{i=0}^{N} X(\tau_i) L_{pi}(\tau) \tag{2.29}$$

where

$$L_{pi}(\tau) = \prod_{j=0, j\neq i}^{N} \frac{\tau - \tau_j}{\tau_i - \tau_j} \tag{2.30}$$

and the interpolating polynomials must satisfy

$$L_{pi}(\tau) = \begin{cases} 1 & for \quad i = j \\ 0 & for \quad i \neq j \end{cases} \tag{2.31}$$

- **Control**. It is approximated by using N Lagrange interpolating polynomials

$$u(\tau) \approx U(\tau) = \sum_{i=1}^{N} U(\tau_i) L^*_{pi}(\tau) \tag{2.32}$$

where

$$L^*_{pi}(\tau) = \prod_{j=1, j\neq i}^{N} \frac{\tau - \tau_j}{\tau_i - \tau_j} \tag{2.33}$$

and the interpolating polynomials must satisfy

$$L_{pi}^{*}(\tau) = \begin{cases} 1 & for \quad i = j \\ 0 & for \quad i \neq j \end{cases} \tag{2.34}$$

By differentiating (2.29), the following expression results

$$\dot{x}(\tau) \approx \dot{X}(\tau) = \sum_{i=0}^{N} x(\tau_i)\dot{L}_{pi}(\tau) \tag{2.35}$$

In order to make a more compact notation, the derivative of the Lagrange polynomials at the LG points can be expressed in a matricial form, by means of

$$D_{ki} = \dot{L}_{pi}(\tau_k) = \sum_{l=0}^{N} \frac{\prod_{j=0,j\neq i,l}^{N}(\tau_k - \tau_j)}{\prod_{j=0,j\neq i}^{N}(\tau_i - \tau_j)} \tag{2.36}$$

Transcribing the dynamic constraint (2.36) into an algebraic constraint

$$\sum_{i=0}^{N} D_{ki}X_i - \frac{t_f - t_0}{2} f(X_k, U_k, \tau_k; t_0, t_f) = 0 \tag{2.37}$$

As the LG points do not cover the initial and final collocation points, they need to be defined

$$X_0 \equiv X(-1) \tag{2.38}$$

$$X_f \equiv X_0 + \frac{t_f - t_0}{2} \sum_{k=1}^{N} \omega_k f(X_k, U_k, \tau_k; t_0, t_f) \tag{2.39}$$

where ω_k are the Gauss weights.

Next, a Gauss quadrature is going to be used to approximate the continuous cost function

$$J = \Phi(X_0, t_0, X_f, t_f) + \frac{t_f - t_0}{2} \sum_{k=1}^{N} \omega_k L(X_k, U_k, \tau_k; t_0, t_f) \tag{2.40}$$

Finally, the boundary constraints and the path constraints are posed in a mathematical form. They take the following expressions

$$\phi(X_0, t_0, X_f, t_f) = 0 \tag{2.41}$$

$$g(X_k, U_k, \tau_k; t_0, t_f) \leq 0 \tag{2.42}$$

Note that, in order to obtain (2.42), the general expression for the path constraint (2.28) has been evaluated at the LG points.

Hence, the definition of the NLP problem is given by the previously defined expressions (2.40),(2.41) and (2.42). The solution of the NLP problem is an approximation to the exact solution of the continuous Bolza problem.

Please refer to [21] in order to get a deeper insight into the mathematical description of the problem, and to obtain the discretized KKT conditions, the discretized necessary conditions and the costate estimate. A comparison of all the optimal control algorithms that are used nowadays can be found on [22].

2.4 Collocation method

As detailed in [25], it is a numerical method in which the state and control functions are represented by piecewise polynomials, and collocation is used to satisfy the differential equations of motion. It is a direct method, which has considerable advantages over simpler direct shooting methods due to the additional constraints imposed. The steps required in order to obtain a solution from the Collocation method are the following ones:

- Firstly, the problem must be subdivided into a sequence of smaller trajectory arcs, referred to as phases.
- For each phase, the interval is subdivided into N segments; as the problem solved has only one phase, the subdivision into segments is directly implemented.
- With this method, a polynomial is defined for each of the segments, taking into account the values of the state and the state time derivatives at the nodes.
- The values of the states are then selected to force the interpolated derivatives to agree with the differential equations at the center of the segments.

This procedure can be visualized in the following depiction

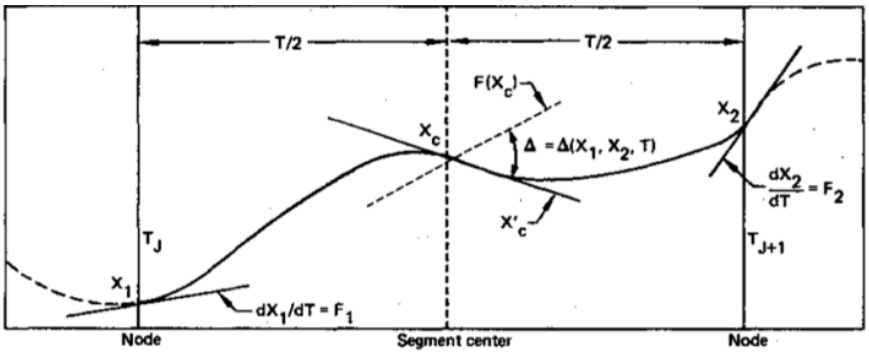

Figure 2.4: Representation of the collocation method applied between two nodes (from [4]).

Therefore, its main difference with the Pseudospectral method is that the latter is based on global interpolation, creating a single polynomial by analyzing all the nodes; the Collocation method, as aforementioned, does construct a polynomial between each pair of nodes. Although this method does require more computational work and time, it can operate with abrupt states and controls.

In order to compute the solution for the Optimal Control Problem solved in this Thesis, the collocation method is used. This is mainly due to the fact that a Bang-Bang control is required, which would imply a discontinuity in the control function that cannot be properly held by the Pseudospectral method. This method would require a smooth control, in order to define a polynomial from analyzing all the nodes; since a Bang-Bang control is obviously discontinuous, it is not feasible to obtain such a polynomial. Since, on the other hand, the Collocation method creates a polynomial for each pair of nodes, the discontinuity present in the control can be handled in a much more efficient way, being this method the most appropriate one for this type of Bang-Bang controls.

2.5 Descent maneuver control

The implementation of the Low-Thrust Optimal Control Problem into GPOPS will be defined in detail in the next section; however, some introductory remarks are made next, in order to provide a first insight into the analysis that is going to be carried out. Four different fields need to be defined in an Optimal Control Problem, as follows

- The dynamical constraints, defined in a Body-Fixed Reference Frame (BFRF) with Cartesian coordinates. The expressions are going to be stated in the next

Chapter, together with an in-depth study of the parameters implemented and the spacecraft propulsive characteristics.

- The control parameter will be the thrust, i.e. it will be the parameter optimized by the GPOPS solver, both in magnitude and direction.
- The initial conditions are set differently for each of the cases; in all of them, the spacecraft is placed at no more than 50 meters from Phobos' surface.
- The final conditions are set depending on the position at which the spacecraft is required to land; it will be, obviously, at a point on Phobos' surface.
- A Path constraint is also introduced, in order for the spacecraft to be placed at all times either on the surface or at a given height above it.

$$r \geq R \tag{2.43}$$

where R is the Phobos mean radius (R = 11.2667 Km).

The solver used is **IPOPS** which can be defined, in words of [23], as a line-search filter interior-point method in which the outer loop approximately minimizes a sequence of non-linearly equality constrained barrier problems for a decreasing sequence of barrier parameters. The inner loop uses line-search filter SQP method to approximately solve each barrier problem. Global convergence is formulated as a barrier problem which is enforced through a line-search filter method, and the filter is reset after each barrier parameter update. The inner iterations include second-order correction steps and a mechanism for switching to a feasibility restoration if the step size becomes to small. The solver has an option for using limited memory BFGS updates to approximate the Hessian of the Lagrangian.

Chapter 3

Description of the problem

In this chapter, the Low-Thrust Optimal Control Problem is going to be defined. The dynamical and path constraint are going to be stated, as well as the value of the constant Phobos parameters and the propulsive technology used.

The problem studied is based on the asteroid landing problem solved by [1]. In order to describe the descent maneuver, two reference frames are defined

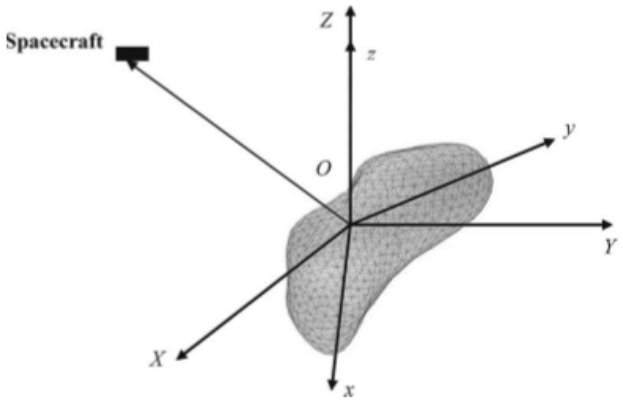

Figure 3.1: Reference frames positioned on Phobos' center (from [1]).

The inertial reference frame is denoted by O-XYZ, while a body-fixed reference frame O-xyz is also attached to the center of Phobos.

The dynamical analysis is based on Newton's Second Law

$$\sum F = ma \tag{3.1}$$

Computing the forces on the body-fixed reference frame O-xyz (hence, accounting for inertial terms), the following expressions are deduced

$$\ddot{x} = 2\omega\dot{y} + \omega^2 x - \frac{\partial U}{\partial x} + \frac{T_x}{m} + \Delta_x \tag{3.2}$$

$$\ddot{y} = -2\omega\dot{x} + \omega^2 y - \frac{\partial U}{\partial y} + \frac{T_y}{m} + \Delta_y \tag{3.3}$$

$$\ddot{z} = -\frac{\partial U}{\partial z} + \frac{T_z}{m} + \Delta_z \tag{3.4}$$

where ω accounts for the magnitude of the angular velocity of Phobos. This parameter can be calculated, assuming circular motion, as follows

$$\omega = \frac{2\pi}{P} \tag{3.5}$$

where P represents the sidereal period. Noting that, for the case of Phobos, $P = 7h, 39.2\, min$, it can be directly deduced that

$$\omega = \frac{2\pi}{27552} = 2.28 \times 10^{-4}\, rad/s \tag{3.6}$$

In the dynamical equations (3.2), (3.3) and (3.4), there also appear the terms Δ_x, Δ_y and Δ_z, which account for the accelerations due to different phenomena, such as

- Solar radiation pressure
- Forces caused by Mars' magnetosphere.
- Forces caused by Phobos' magnetosphere.
- Sun's gravitational perturbations.

As these phenomena are still under investigation [6], they have not been included into the analysis.

There are other parameters that need to be introduced into the study. The ones used are from [26], a relatively recent analysis that provides a considerable refinement over previous studies [27]. In particular, the density and the gravitational parameter take the following values

- Density of Phobos. $\rho_{Ph} = 1876 \pm 20\, Kg/m^3$.
- Gravitational Parameter. $GM = 0.7127 \pm 0.0021 \times 10^{-3} Km^3/s^2$.

3.1 Propulsion technology

Electric propulsion is going to be used to boost the spacecraft. One of the most representative figures in this type of propulsion is the thrust efficiency, defined in [28] as

$$\eta_T = \frac{FI_{sp}}{2P} \tag{3.7}$$

Electric propulsion is power-limited, since the input power comes from an external electric power source. Hence, a trade-off must be made between thrust and specific impulse. As it is required that the I_{sp} must be as large as possible, it can be directly deduced from (3.7) that the thrust must be small.

Electric propulsion (EP) thrusters are classified, according to the acceleration mechanism used, as follows

- Electrothermal thrusters.
- Electrostatic thrusters.
- Electromagnetic thrusters.

Please refer to [28] in order to have a detailed description of the different thrusters available within each of the EP thruster families itemized. For the mission analyzed, a Hall effect thruster is going to be used.

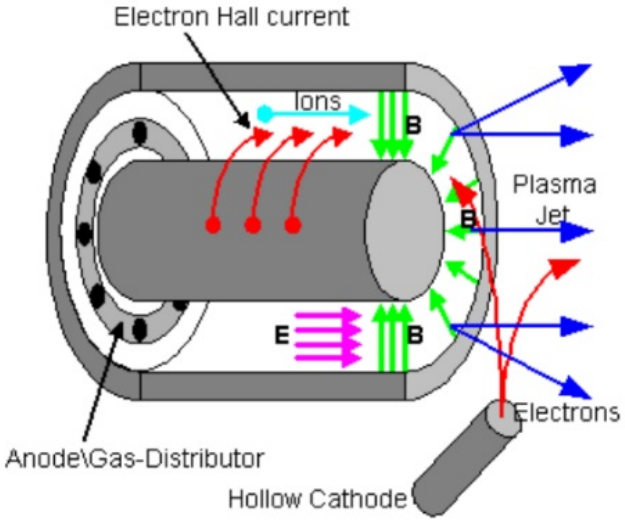

Figure 3.2: Hall Effect Thruster (HET) functioning.

The HETs functioning process takes the following steps

- First, electrons are emitted from the cathode, placed outside of the DC discharge chamber, and they head towards the anode, which is placed on the chamber rear wall.
- While traversing the chamber, they ionize the neutral gas inside of it, creating a plasma.
- The ions created head obviously towards the outside; however, in order to avoid them losing momentum due to random crashes with the electrons, a radial magnetic field is applied, which causes the latter to gyrate, causing an axial force.
- Finally, it must be noted that there must be neutralized plasma at the exit; for this to occur, the outside cathode does also expel electrons towards the ion beam.

As it is described in [28], there are other EP thrusters that provide a higher I_{sp}; for instance, the *Gridded ion thrusters* (GITs). However, HETs have a main advantage compared to GITs: they can achieve higher thrust levels with smaller voltages and a smaller front area. Moreover, they can operate in a broad range of powers. Although low thrust levels are required for this descent maneuver, an HET is required to be introduced, since it can work with no grids; this implies that the dimensions of the front area will be smaller, and the complete propulsive mechanism will be simpler. Moreover, a HET is much lighter than a GIT, a fundamental issue when studying the total Delta-V required for the complete mission.

Two of the most successful HETs operated models can be taken as a reference, with a brief description of each of them addressed next

- **SPT-100 thruster**. It was introduced in the USSR, in 1982. According to [29], its nominal operating conditions were
  - Thrust. 83 mN.
  - Specific Impulse. 1600 s.
- **Snecma PPS-1350-G Hall thruster**. It was the thruster used in the ESA SMART-1 spacecraft. It could be operated with different settings of power, thrust and I_{sp}. According to [30], the working range of each of the three main propulsive parameters were

– Thrust. 30-70 mN.

– Specific impulse. 1100-1600 s.

– Discharge power. 0.46-1.19 KW.

It must be noted, however, that in this mission only the landing maneuver is analyzed; hence, the thrust that is going to be set as a maximum will take a lower value than the values that the previous spacecrafts presented. The technological progress made in the last three decades has allowed, on the other hand, to obtain larger values for the specific impulse. Hence, the values of the propulsive parameters inputted into GPOPS are the following ones:

- Maximum Thrust. 1 mN.
- Specific Impulse. 2000 s.

Note that, although realistic values are implemented into the analysis, no greater insight was made when accounting for existing models, since a feasible mission to Phobos is not expected to occur for at least the next decade [7].

Finally, the thrust vector must be referred to the reference frame defined in Figure 3.1. As described in Section 2.5, both the thrust magnitude and direction are parameters to be optimized; hence, the thrust vector direction can be stated as a function of the two angles represented next,

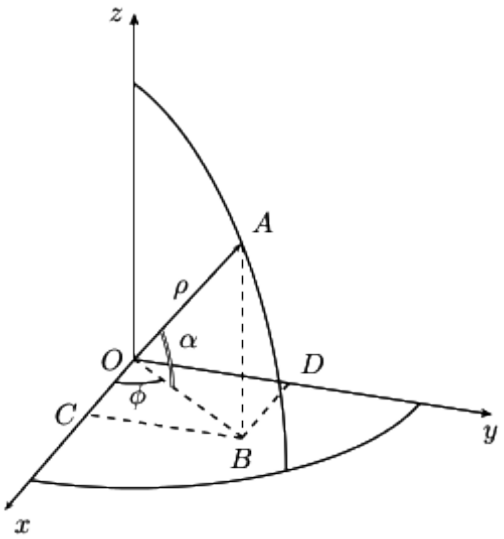

Figure 3.3: Angles used to define the Thrust direction.

As it can be readily observed, the thrust components can be defined as follows

$$T_x = T\, cos(\alpha) cos(\phi) \tag{3.8}$$

$$T_y = T\, cos(\alpha) sin(\phi) \tag{3.9}$$

$$T_z = T\, sin(\alpha) \tag{3.10}$$

Therefore, the thrust magnitude T and the angles that define the thrust direction, (θ, ϕ), will be the parameters to be optimized.

3.2 Departure Orbit

The orbit that the spacecraft follows when approaching Phobos before starting the landing maneuver must be also discussed, since it will affect the initial altitude from which the landing maneuver starts. Four different types of orbits can be analyzed, namely:

- Lyapunov orbits.
- Vertical orbits.
- Halo orbits.
- Distant Retrogade Orbits (DROs)

The first three types are centered on the Lagrange Points L1 and L2. Note that L1 is located 3.5 Km from Phobos' surface; a short descent maneuver with little propellant would be feasible to be made in the case the spacecraft is placed in that position [2]. Moreover, the radiation exposure that the spacecraft sustains would be greatly reduced, because both Phobos and Mars would act as a shield.

These orbits have, nonetheless, a major drawback: they are unstable, oscillating in-plane, out-of-plane and both in- and out- of plane. Note that instability is primarily referred to the quickness a trajectory will depart from its nominal orbit when being perturbed, without the aid of orbital maintenance maneuvers [5].

On the other side, the DROs do combine three very important aspects, namely: that they can be performed at low altitude, they do not need a significant propellant expenditure when performing orbital maintenance maneuvers, and they are intrinsically stable.

Moreover, an additional advantage can be obtained by inclining a DRO: a significant perturbation will not imply an along-track departure [2]. As aforementioned,

DROs can be also performed at low altitudes (around 20 Km), which would reduce the Delta-V required, as well as increasing the radiation shielding. They have, nonetheless, a major drawback: there is a great relative velocity to be compensated if a landing is performed when the departure orbit is a DRO. Therefore, a trade-off analysis must be performed when analyzing the complete mission. As a final remark, it must be noted that the accuracy of the navigation instruments becomes crucial when decreasing the altitude, as the probability of a surface crash increases; hence, improvements in this field have a direct beneficial consequence on the landing maneuver analyzed.

After having stated all the parameters, as well as the propulsive technology used, the Low-Thrust Optimal Control Problem can be formally posed as follows

Minimize the cost functional

$$J = \int_0^{t_f} T(t)dt \tag{3.11}$$

subject to the dynamic constraints

$$\ddot{x} = 2\omega\dot{y} + \omega^2 x - \frac{\partial U}{\partial x} + \frac{T_x}{m} + \Delta_x \tag{3.12}$$

$$\ddot{y} = -2\omega\dot{x} + \omega^2 y - \frac{\partial U}{\partial y} + \frac{T_y}{m} + \Delta_y \tag{3.13}$$

$$\ddot{z} = -\frac{\partial U}{\partial z} + \frac{T_z}{m} + \Delta_z \tag{3.14}$$

and the boundary conditions

$$x(0) = x_0 \tag{3.15}$$

$$x(t_f) = x_f \tag{3.16}$$

$$y(0) = y_0 \tag{3.17}$$

$$y(t_f) = y_f \tag{3.18}$$

$$z(0) = z_0 \tag{3.19}$$

$$z(t_f) = z_f \tag{3.20}$$

where the coordinates defining the final position must fulfill that

$$\sqrt{x_f^2 + y_f^2 + z_f^2} = R \tag{3.21}$$

and the following path constraints needs to be satisfied all over the trajectory

$$r \geq R \tag{3.22}$$

For the velocity magnitude, the boundary conditions will be formulated as follows

$$\dot{x}(0) = \dot{x}_0 \tag{3.23}$$

$$\dot{x}(t_f) = \dot{x}_f \tag{3.24}$$

$$\dot{y}(0) = \dot{y}_0 \tag{3.25}$$

$$\dot{y}(t_f) = \dot{y}_f \tag{3.26}$$

$$\dot{z}(0) = \dot{z}_0 \tag{3.27}$$

$$\dot{z}(t_f) = \dot{z}_f \tag{3.28}$$

where the final velocity components do always take for this analysis

$$\dot{x}(t_f) \equiv \dot{y}(t_f) \equiv \dot{z}(t_f) = 0 \tag{3.29}$$

and the velocity magnitude is represented as follows

$$|\vec{V}| = \sqrt{\dot{x}^2 + \dot{y}^2 + \dot{z}^2} \tag{3.30}$$

Note that, in the subsequent analysis, the imposed Boundary Conditions (BC) for both the position and the velocity take the same limits as the initial and final values defined in (3.16), (3.18), (3.20) and (3.24), (3.26), (3.28), respectively. This implementation is chosen for the purpose of making the solver work in a more efficient way; if the BC covered a larger area, the solver would still find the optimal solution, but requiring more computational time.

The Bang-Bang control used has, for the magnitude part, the following limits

$$T_{min} = 0\,\mathrm{N} \tag{3.31}$$

$$T_{max} = 10^{-3}\,\mathrm{N} \tag{3.32}$$

whereas the direction of the thrust is defined, as aforementioned, by two angles (Figure 3.3), with limits

- For the azimuth angle ϕ

$$\phi_{min} = 0\, rad \tag{3.33}$$

$$\phi_{max} = 2\pi\, rad \tag{3.34}$$

- For the elevation angle α

$$\alpha_{min} = -\pi/2\, rad \tag{3.35}$$

$$\alpha_{max} = \pi/2\, rad \tag{3.36}$$

Chapter 4

Results

4.1 Introductory remarks

As aforementioned in the introduction to this Thesis, a descent maneuver to the Phobos' surface modeled as a Low-Thrust Optimal Control Problem is going to be computed using the program GPOPS. In order to make a more accurate analysis, the gravity acceleration is computed by the Polyhedron method developed by [16], based on Werner's study [3]. In the final part of this Chapter, the results obtained are presented, together with a discussion in which a description of the depictions provided is made from a physical point of view.

4.2 Computational work developed

The process followed was

- Firstly, the body constants for which the Polyhedron method gave the acceleration were inputted into GPOPS, being the ones defined in Chapter 3. A Phobos shape file was then loaded, with the shape defined by the vertices and faces; different files were available [31], depending on the level of detail with which the volume is characterized. In principle, the file that gives a more precise shape should be the one implemented; however, this comes at the expense of more computational time. Hence, a trade-off was made, assuming that the computational resources were limited.

- Then, the Optimal Control Problem, with its dynamic (3.12), (3.13), (3.14) and path constraints (3.22), was implemented in GPOPS; the thrust and specific impulse values specified in Chapter 3 were also included into the analysis.

- The codes for both the gravity computation and the optimization problem were arranged in such a way that the exact value of the gravity parameter entered into the dynamical equations, i.e. the exact gravity value at the point at which the spacecraft was placed at every instant was inputted into the GPOPS solver, which analyzed the complete trajectory through the collocation method. The total number of points at which the polyhedron code should compute the gravity acceleration was predetermined in the GPOPS problem, by adjusting the number of nodes.

- Finally, the initial conditions were implemented for each of the problems analyzed.

This method is very precise, in the sense that only the intrinsic error of the Polyhedron method enters into the computations, and it reduces substantially the dynamics' uncertainty. It is, nonetheless, unfeasible, due to the limited computational resources.

There were also problems concerning the Phobos shape model. The file with the lowest amount of vertices and faces could not be used with the code structure defined by [16] since, as explained in Chapter 2, a Link-check function had to prove whether a given edge, defined by its two vertices, had been already analyzed or not, thus consuming a lot of memory. Even with the new equipment acquired (a 16 GB RAM computer), the code did not have enough memory to check each of the polygon edges that constituted the Phobos shape; around 40 GB of RAM memory are estimated to be required in order to be able to compute the gravity acceleration caused by Phobos with the Polyhedron method code developed by [16].

Hence, the code structure was changed. The previous code [16] was designed for the computational time to take priority over the memory resources, a factor that is an advantage when computing the acceleration for small bodies; for the asteroid Castalia, the code could compute the acceleration at any point outside the body in five seconds. When analyzing much larger bodies, nonetheless, the memory resources required were unfeasible, as aforementioned. Therefore, a new code concerning the edge-storing matrix was developed, being structured as follows

- A Link Check matrix is firstly defined, in which each row accounts for an edge; hence, the matrix will have two columns, accounting for the two vertices required to define an edge.

- Each edge was compared against all the polyhedron edges present in the Link Check matrix, comparing whether the edge had been already stored or not. As explained in Chapter 2, the edge that two polygons share cannot be treated as two different edges; note that the initial and final vertices' values of a given edge will be the opposite for the two contiguous faces. In fact, the initial vertex that defines the edge as analyzed from face 1 will be the final vertex of the edge when defined from face 2, with the same reasoning for the other vertex.

  It must be pointed out that the comparison between the current edge analyzed and the edges already present in the matrix is made in such a way that the counter only goes through the already filled edges (rows in the Link Check matrix), and not through all the matrix rows for all the edges analyzed. This minor detail allows to save a lot of computational time, especially when the first edges are analyzed, with almost all the matrix rows empty.

- Both the normals to the faces and the Dyads are computed as explained in Chapter 2, in a similar trend to that employed by [16].

The computational time was reduced to one hour and a half, processing the data with a 16 GB RAM computer. Although it represents a very large computational time, it must be noted that memory was the primordial aspect to be reduced in this case, at the expense of this computational time; besides, this computation has to be carried out only once for a given body analyzed (Phobos in this case). When including this new code into the general Polyhedron code, the gravity computation could be made with this 16 GB computer, while with the approach taken by [16], 40 GB were required, as aforementioned. In the latter, obviously, the optimization of the computational time was much better, as no memory constraints were introduced.

Although this new code was useful to process the Phobos shape data file and obtain the gravity acceleration for a given position vector, the first approach made was not feasible, i.e. in which this gravitational code gives the gravity acceleration value for each of the nodes defined in the spacecraft trajectory in GPOPS; this approach would require much more computational resources, in order for the GPOPS code to call the Polyhedron code for each of the spacecraft nodes analyzed. Hence, an interpolation method was developed, consisting in the following guidelines

- A mesh is defined in 3 dimensions. The number of points constituting it is selected in correlation with the number of nodes in which the surface is discretized; in this way, each of the spacecraft trajectory points has two points

within a distance of one meter , having the selected points an acceleration value defined (obtained from the Polyhedron code). The acceleration grid would then take a cube shape in a coordinate system, with internal surfaces of acceleration points obtained for a point of the third coordinate analyzed. A set of values for this analyzed axis are stated, thus creating the different surfaces of acceleration points. Note that the axis analyzed, the one that is orthogonal to the surfaces created, is set so that one of the acceleration components will go through this direction.

For instance, if the z-coordinate is analyzed, a set of surfaces are created, with each one covering the entire values of the x and y coordinates for a constant value of z; each surface (represented in MATLAB as a matrix) will account for each of the values of z defined. Note that the chart obtained (the structure in which all the matrices are encapsulated), will represent the acceleration table for the a_z component, as aforementioned. This same procedure is carried out for the two other coordinates.

- Having defined the mesh, the modification of the gravity code [16] is used to calculate the acceleration value at each of those points, just by setting the position vector.

- Finally, an interpolating function is derived for each of the three coordinates, relating the point at which the gravity is required to be known with the ones at which the gravity value has been pre-established; the cubic-spline method, since this method fits a different cubic polynomial between each pair of data points for curves, or between sets of three points for surfaces. In this way, for each of the trajectory points (nodes) of the spacecraft, the previous code will obtain the value of the three components of the acceleration by using the previously derived interpolating functions.

Using this approach, the time needed for the GPOPS iteration process to converge was shortened, thus making the resolution of the problem stated feasible. There is, however, a major disadvantage when computing the acceleration by means of an interpolating function: there is an intrinsic error in the acceleration calculation as compared with the much more precise Polyhedron method. This error can be computed as follows

- The acceleration vector is calculated by the two methods (the Polyhedron method and the interpolation method) at an interval of points, chosen so that the spacecraft trajectory is encapsulated among those points.
- The vector difference between the acceleration vectors using the two methods at each point is calculated. The computation is repeated for all the nodes analyzed.
- The norm of the vector difference at each node is computed.
- The norms from all the nodes are added.

The previous explanation can be posed mathematically as follows

$$\epsilon = \sum_{i}^{N} |\vec{g}_{i,p} - \vec{g}_{i,in}| \tag{4.1}$$

where $i = 1, ..., \mathrm{N}$, with p accounting for the polyhedron method and in for the interpolation method.

The reason by which the error will be different depending on the number of points is straightforward: the greater the number of points, the more accurately defined will the mesh be. This will imply that, when the acceleration is computed, the interpolation method will give values closer to the ones obtained with the Polyhedron method.

There is, however, a major inconvenience that arises when increasing the number of points: the computational time increases as well. Hence, this parameter must be chosen so that the error is the lowest possible, with the lowest amount of computational time for that error. Therefore, the evolution of the error with the number of points is depicted, and can be appreciated below.

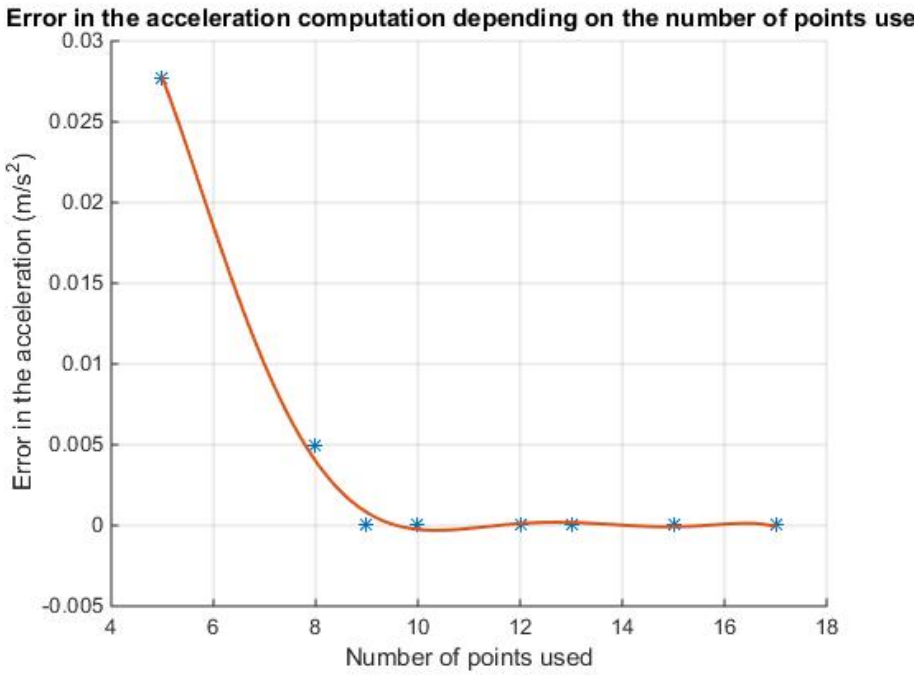

Figure 4.1: Error in the acceleration computation as a function of the number of points used to define the mesh.

As can be observed in Figure 4.1, the error takes a large value when less than eight points are chosen. From then on, the error difference when increasing the number of points is very small.

The previously represented error is, however, an absolute error, since it does not take into account how big is the error committed as compared to the set of data analyzed. Hence, the relative error is the next parameter analyzed, giving an indication of how good a measurement is relative to the set of data that enters into the computation. In particular, the average relative error is analyzed next, which takes the following expression

$$\epsilon_{rel} = \frac{1}{N} \sum \frac{\epsilon}{|\bar{a}|} \tag{4.2}$$

Where N refers to the number of points used to define the mesh. As in the previous case, the evolution of the error (in this case relative) as a function of the number of points used to define the mesh is represented

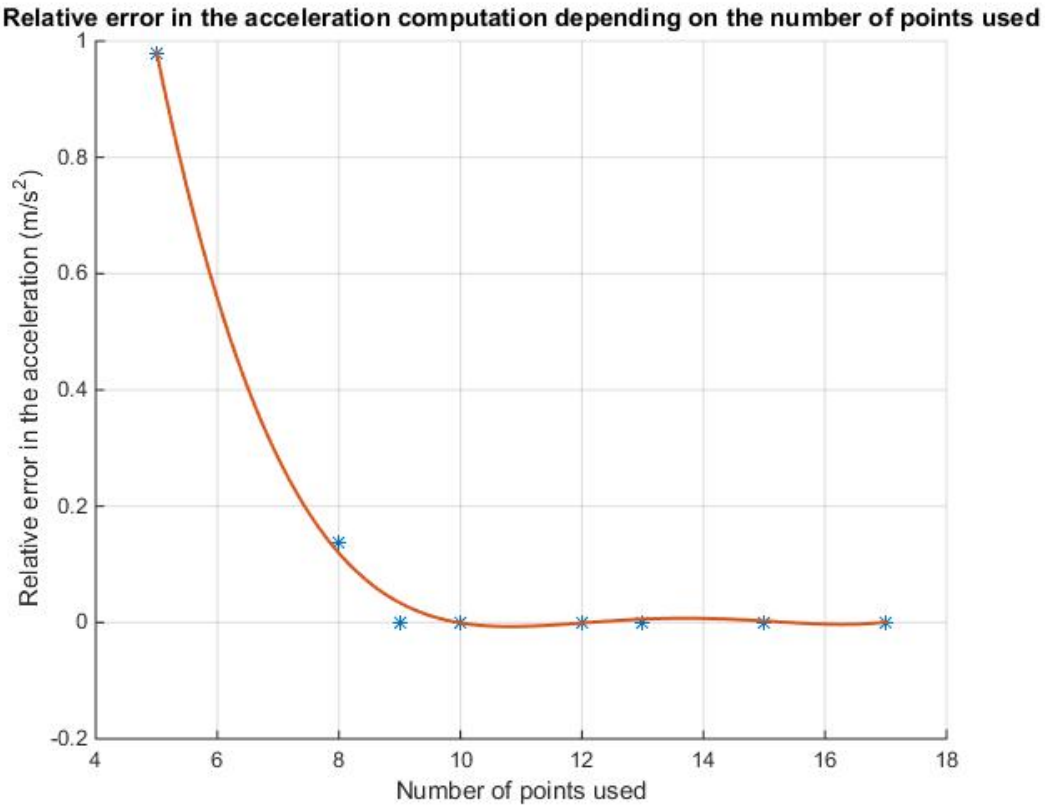

Figure 4.2: Relative error in the acceleration computation as a function of the number of points used to define the mesh.

There is, however, a major problem when computing the relative error for a wide interval of points, i.e. that increasing the number of points from a value at which the relative error is very small produces differences in relative error that cannot be fully appreciated; as observed in Figure 4.2, for a number of points from 9 to 17, the interpolation curve follows an asymptotic trend. Therefore, a logarithmic representation of the relative error in the acceleration is also depicted, showing in more detail the differences between the number of points used in the asymptotic branch

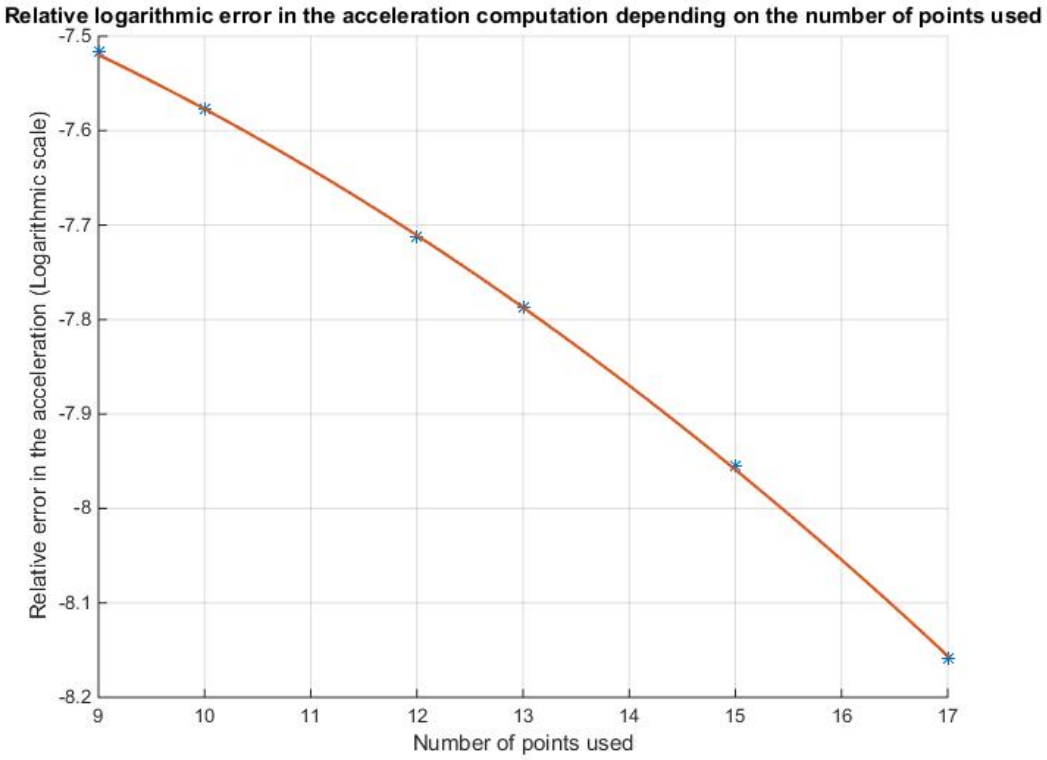

Figure 4.3: Logarithmic representation of the relative error in the acceleration computation as a function of the number of points present in the asymptote observed in Figure 4.2

There are appreciable differences in the relative error for a larger number of points used, as observed in Figure 4.3. When using a number of points N = 9, the relative error order of magnitude (in m/s^2) is $\mathcal{O} \sim 10^{-4}$ whereas for almost two times this number of points, N = 17, the error committed is $\mathcal{O} \sim 10^{-5}$ (note that, in Figure 4.3, the relative error is represented in logarithmic scale). Hence, although it is obvious that more precision could be obtained with a larger number of points, it seems reasonable to define the mesh with a number of points N = 9, since a good accuracy can be obtained with a relatively short computational time.

Having defined the acceleration method used, the discussion of the results for the Low-Thrust Optimal Control Problem analyzed is addressed next. The problem has been solved numerically, and two methods are available in order to obtain the solution of the dynamical constraints defined in (3.2), (3.3) and (3.4). As explained in Section 2.4, the collocation method is the method used, since it is able to deal with the discontinuity in the control function caused by the Bang-Bang control desired, an aspect that cannot be properly held by the Pseudospectral method.

When computing the problem in GPOPS with the Collocation method, the solution converged. Therefore, the three main parameters that define the spacecraft operation are discussed next

- **Position.** Although the problem is solved in GPOPS in Cartesian coordinates (with the dynamical constraints present in equations (3.2), (3.3) and (3.4)), a representation of the radial position is preferable, in order to assure that the path constraint presented in (3.22) is fulfilled; i.e. ascertain than, for all instants of time, the radial position at which the spacecraft is placed is greater than the radius of the body analyzed. The conversion from Cartesian coordinates is straightforward

$$r = \sqrt{x^2 + y^2 + z^2} \tag{4.3}$$

  The results presented below are based on a landing maneuver with the following initial and final conditions for the position

  - **Initial Conditions**.

$$x_0 = \frac{R + 30}{\sqrt{3}}\, m \tag{4.4}$$

$$y_0 = \frac{R + 30}{\sqrt{3}}\, m \tag{4.5}$$

$$z_0 = \frac{R + 30}{\sqrt{3}}\, m \tag{4.6}$$

  - **Final Conditions**

$$x_f = \frac{R}{\sqrt{3}}\, m \tag{4.7}$$

$$y_f = \frac{R}{\sqrt{3}}\, m \tag{4.8}$$

$$z_f = \frac{R}{\sqrt{3}}\, m \tag{4.9}$$

  The resulting evolution of the spacecraft radial position as time advances can be appreciated in the following image

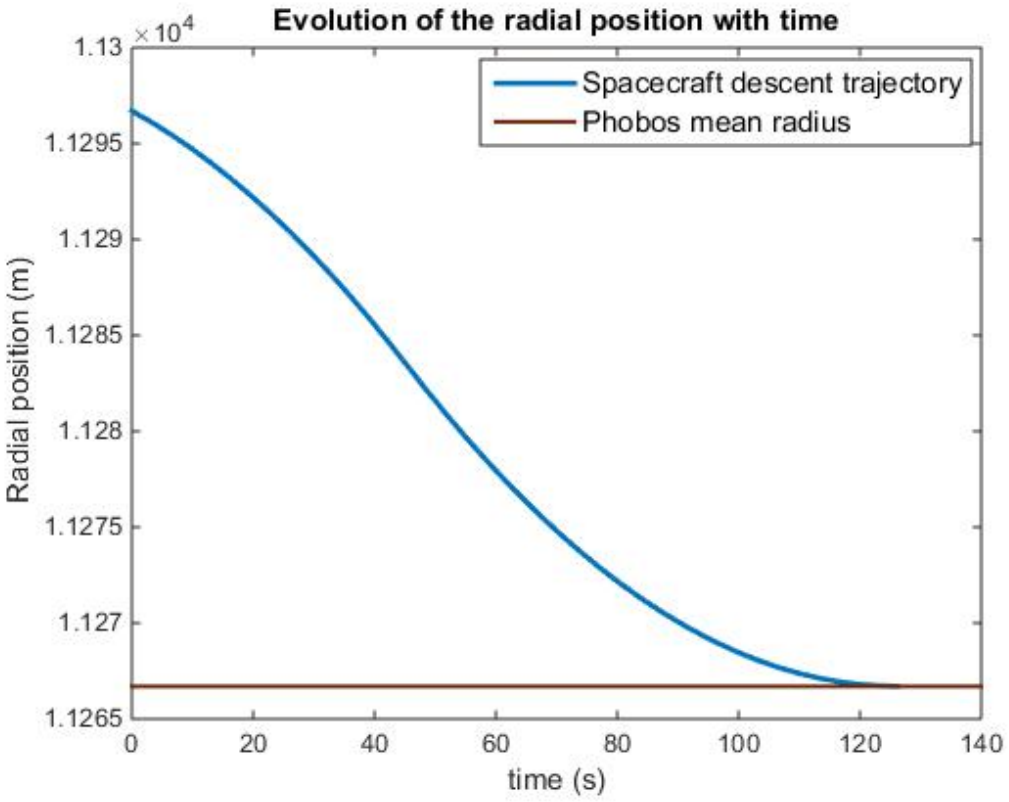

Figure 4.4: Evolution of the spacecraft radial position with time.

As can be observed in Figure 4.4, the radial distance from the Phobos' center decreases with time, until the spacecraft reaches the surface. Hence, it has been proven that the Optimal Control Problem has been solved successfully, since the GPOPS solver has converged to the point required on Phobos' surface.

- **Velocity.** In the same fashion, the module of the velocity is represented as

$$|\vec{V}| = \sqrt{V_x^2 + V_y^2 + V_z^2} \tag{4.10}$$

The initial conditions and final conditions for the velocity magnitude are

  - **Initial Conditions**.

$$\dot{x}_0 = -0.1\, m/s \tag{4.11}$$

$$\dot{y}_0 = -0.1\, m/s \tag{4.12}$$

$$\dot{z}_0 = -0.1\, m/s \tag{4.13}$$

– **Final Conditions**

$$\dot{x}_f = 0\, m/s \tag{4.14}$$

$$\dot{y}_f = 0\, m/s \tag{4.15}$$

$$\dot{z}_f = 0\, m/s \tag{4.16}$$

In case a specific velocity component in spherical coordinates is required to be represented, the following expressions have been also implemented

$$\vec{V} = \vec{V_r} + \vec{V_\theta} + \vec{V_\phi} \equiv \dot{r}\, \vec{e}_r + r\dot{\theta} cos\phi\, \vec{e}_\theta + r\dot{\phi}\, \vec{e}_\phi \tag{4.17}$$

with the magnitude being

$$|\vec{V}| = \sqrt{V_r^2 + V_\theta^2 + V_\phi^2} \tag{4.18}$$

where θ is the azimuth angle and ϕ is the elevation angle.

In the following depiction, however, the evolution of the velocity module has been the magnitude depicted. No velocity components have been represented, since the most interesting phenomenon that needs to be analyzed is the evolution of the velocity depending on whether the thrust is turned on or off, an issue treated subsequently.

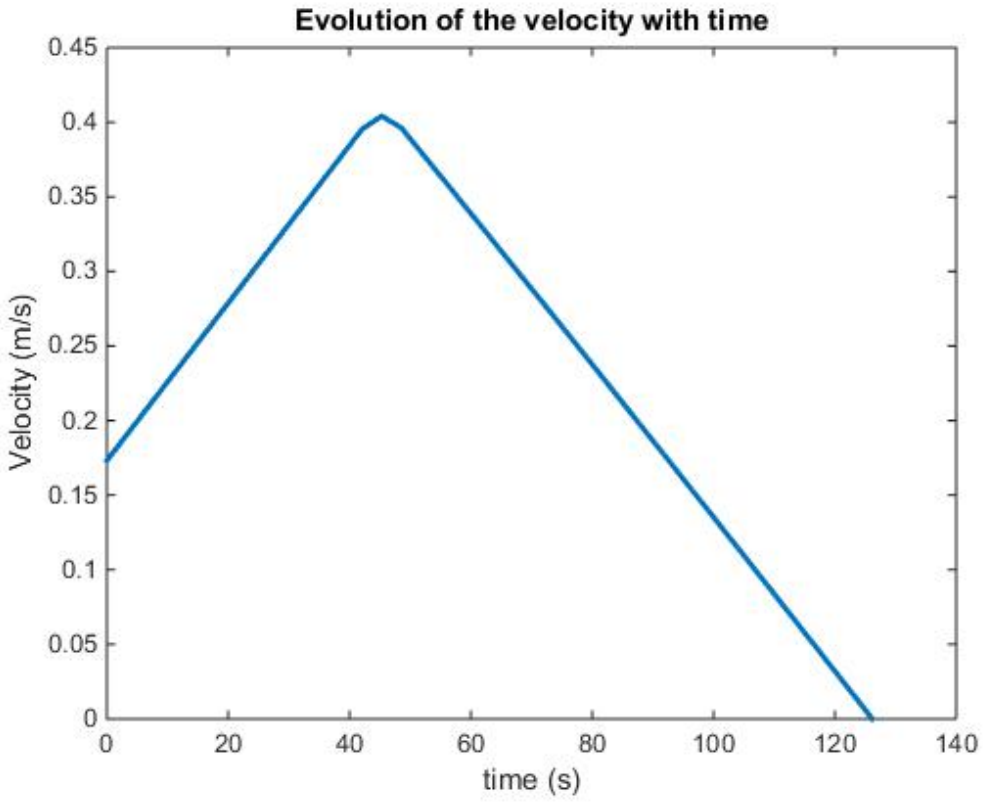

Figure 4.5: Evolution of the velocity module with time.

As can be appreciated in Figure 4.5., the velocity will increase linearly until an approximate time of 42 seconds. From then on, it will decrease in the same trend, linearly, until it will go to zero at a time larger than 120 seconds. Note that, since the acceleration is the derivative of the velocity with respect to time, the previous explanation makes total sense; due to the increase in the acceleration module until a time equal to 42 seconds, an increase in the velocity module will be obtained too.

- **Thrust magnitude.** The magnitude of the thrust parameter is also represented. It is modeled as a Bang-Bang control, with the following results obtained

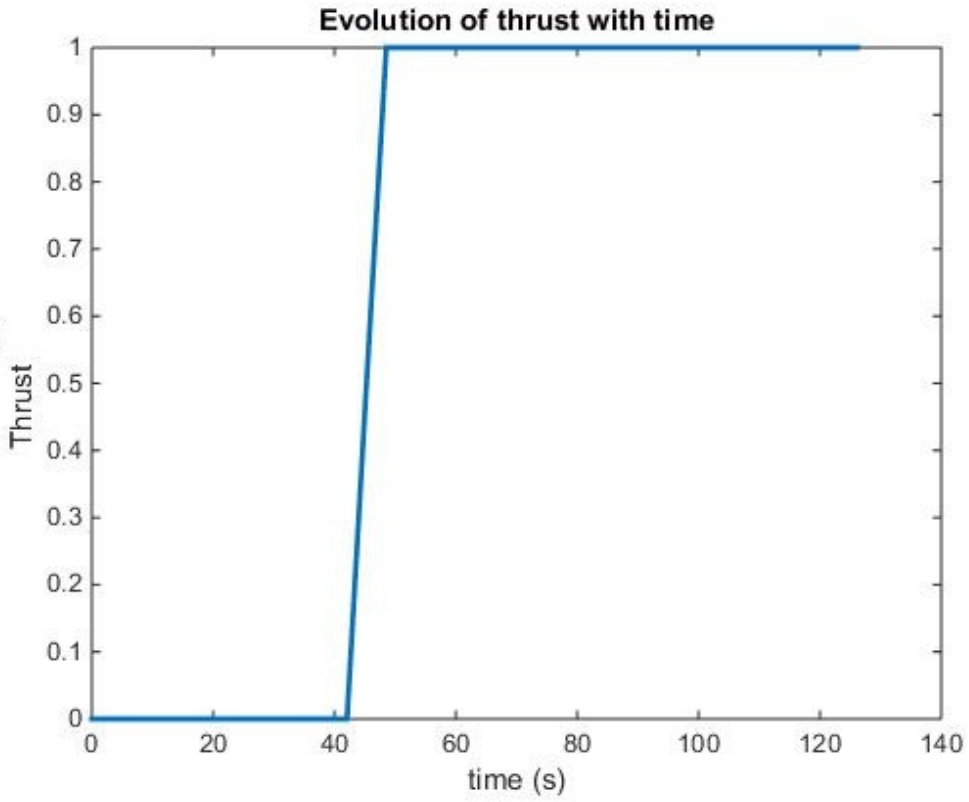

Figure 4.6: Evolution of the thrust magnitude with time.

As can be observed in Figure 4.6, a Bang-Bang control has been obtained. The physical phenomena occurring is straightforward. There is null thrust up to 40 seconds; in this case, the velocity increases due to the gravitational attraction that Phobos exerts on the spacecraft. From that point on, the thrust is increased to a maximum and directed in the opposite direction to the spacecraft motion, in order to make it lose velocity progressively, until it finally stops when touching the surface. This phenomena completely correlates with the velocity evolution in Figure 4.5, since the velocity will increase when no thrust is applied, thus being attracted to Phobos; when the thrust is turned on and used as a brake, the velocity will progressively decrease, until reaching zero at the Phobos surface. As a final remark, it must be pointed out that the velocity in Figure 4.5 takes a value equal to zero at exactly the same time at which the radial position of the spacecraft equals the Phobos' radius, which proves that the velocity constraint imposed on the Optimal Control Problem is fulfilled, i.e. that at the precise instant of time at which the spacecraft touches Phobos' surface, the velocity has to be equal to zero.

4.3 3D Landing Maneuver

The previously discussed results have demonstrated the validity of the model, since an optimal control solution was found. Next, the Low-Thrust Optimal Control Problem is going to be tested for another initial condition in the position. Note that the ones defined for the previous problem (equations (4.4), (4.5) and (4.6)), together with the final position conditions (expressions (4.7), (4.8) and (4.9)) represented a straight-line descent maneuver in the radial direction, for which the GPOPS solver can find an optimal solution more easily. In the next simulation, nonetheless, the initial conditions implemented do not define a point in the radial direction, so that the GPOPS solver should be sufficiently robust in order to find the optimal solution by adjusting the control, i.e. the thrust magnitude.

Hence, the initial conditions for the position in this case are

- **Initial Conditions**.

$$x_0 = \frac{R+20}{\sqrt{3}}\, m \tag{4.19}$$

$$y_0 = \frac{R+30}{\sqrt{3}}\, m \tag{4.20}$$

$$z_0 = \frac{R+15}{\sqrt{3}}\, m \tag{4.21}$$

- **Final Conditions**. The final conditions will be the same as in the previously analyzed case.

$$x_f = \frac{R}{\sqrt{3}}\, m \tag{4.22}$$

$$y_f = \frac{R}{\sqrt{3}}\, m \tag{4.23}$$

$$z_f = \frac{R}{\sqrt{3}}\, m \tag{4.24}$$

The initial and final conditions for the velocity parameter are the same as in the previous case, with the former defined in (4.11), (4.12) and (4.13) and the latter defined in (4.14), (4.15) and (4.16).

The new initial conditions for the position were implemented into GPOPS, with the problem converging to an optimal solution. The following results were obtained

- **Position**. The radial position is represented, in order to assure that the spacecraft lands on Phobos' surface.

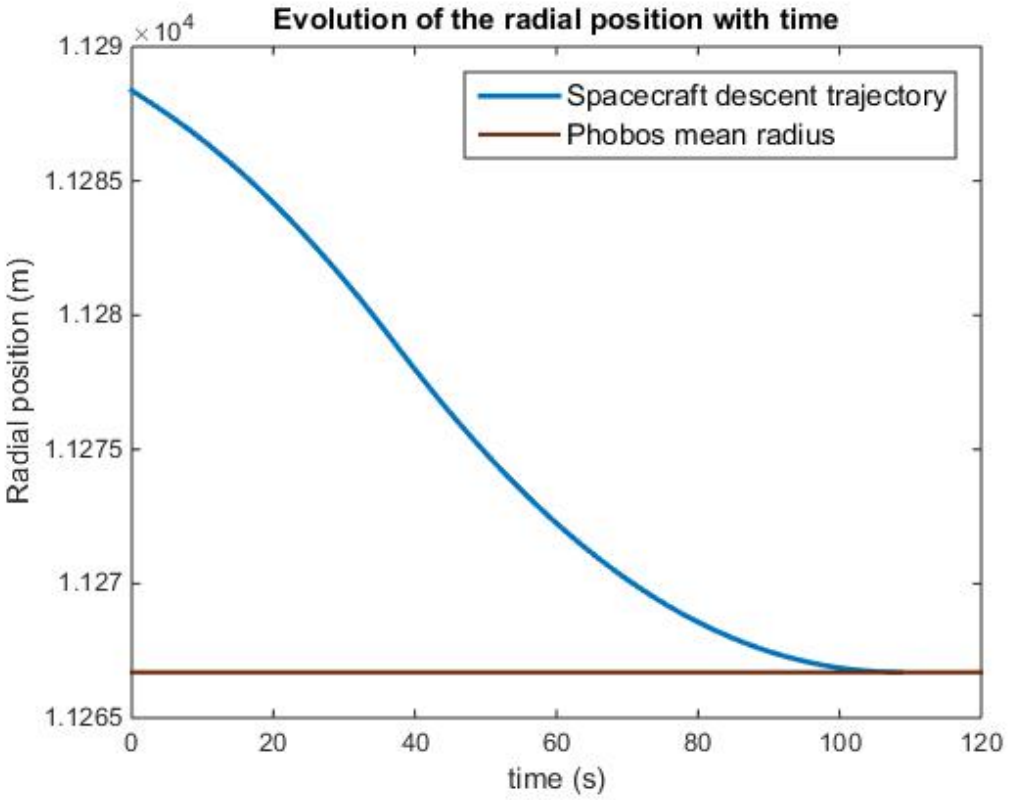

Figure 4.7: Evolution of the spacecraft radial position with time.

As can be appreciated, both the initial and final conditions regarding the position were fulfilled, with the spacecraft landing on Phobos' surface.

- **Velocity and Thrust magnitude**. These two magnitudes are represented together, in order to compare the variation of the velocity magnitude when the thrust magnitude changes.

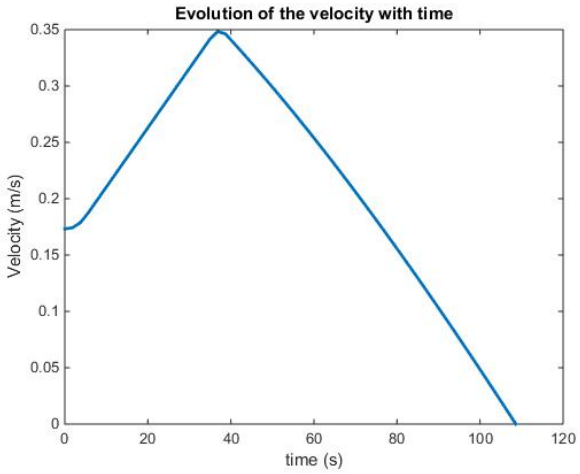

Figure 4.8: Variation of the velocity magnitude with time.

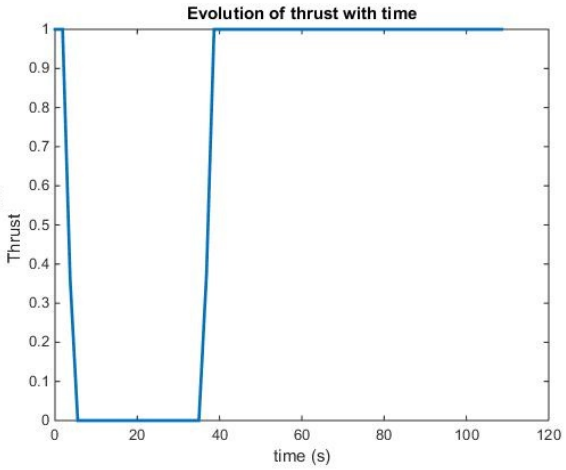

Figure 4.9: Variation of the thrust magnitude with time

As can be observed in the previous image, a thrust correction is made when starting the descent maneuver, with the velocity keeping an approximately constant value during that period. Once the descent trajectory has been fixed, the thrust is turned off, with the velocity increasing due to the gravitational attraction that Phobos exerts on the spacecraft. Note that, in the thrust depiction, an engine thrust ratio has been represented, which can be defined as follows

$$Engine\,Thrust\,Ratio = \frac{T}{T_{max}} \tag{4.25}$$

Hence, when this parameter takes a value equal to 1, the thrust that the HET provides to impel the spacecraft is the maximum one, i.e. $T = T_{max}$; on the other hand, the expression (4.25) taking a value equal to zero will thereby result in zero thrust, i.e. $T = 0$.

Finally, the thrust is turned on again, in order to slow down the spacecraft. Since the thrust magnitude when being fully turned on is greater than the gravitational attraction that Phobos exerts on the spacecraft, the velocity will be progressively reduced, reaching a zero value when the spacecraft touches the Phobos surface. Note that the time at which the velocity takes a zero value is the same one for which the radial position of the spacecraft is equal to the radius, as observed in Figure 4.7. Therefore, the optimality conditions have been fulfilled, with the spacecraft touching the ground at the point required, and at zero velocity.

- **Thrust magnitude comparison between the two cases**. Finally, it is interesting to compare the different actuation of the control for the two cases studied. It can be observed as follows

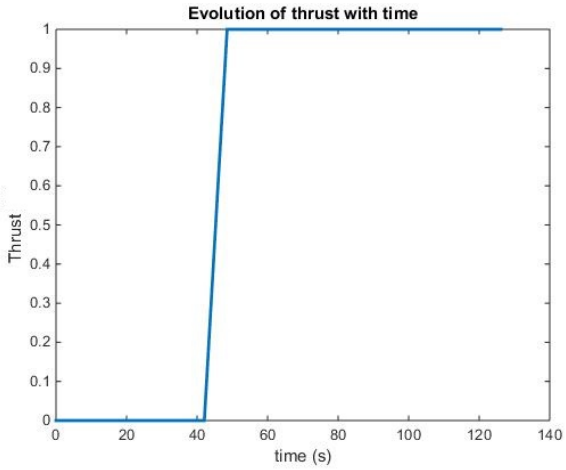

Figure 4.10: Variation of the thrust magnitude with time for the first case.

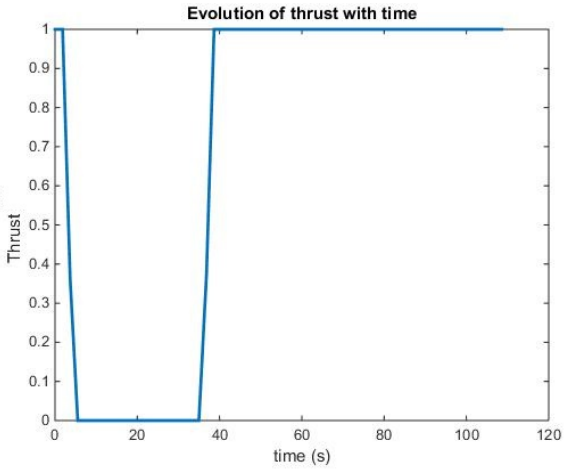

Figure 4.11: Variation of the thrust magnitude with time for the second case.

As aforementioned, the left depiction presented in Figure 4.10 represents the thrust magnitude evolution for the first case, in which an initial radial position has been implemented as initial condition for the position; the right image, on the other hand, represents the second case studied, for which the initial point from which the spacecraft departs is not placed in the radial direction.

The main difference between both cases is the thrust correction that should be made in the second case when starting the descent maneuver, in order to place the spacecraft in the radial direction. As the spacecraft does already depart from a radial position in the first case, no initial thrust correction is required. Once this correction has been made, the thrust is turned off, for the spacecraft to gain velocity due to the Phobos' gravitational attraction. Then, the thrust is turned on to slow down the spacecraft motion, touching Phobos' surface with zero velocity.

As a final remark, note that the time it takes in the second case to perform the complete maneuver is lower than the one required for the first one. This is just because the second initial point (the one not being in the radial direction) is closer to the surface than the first one. Hence, even accounting for the time required for the correction to be carried out, the total maneuver time is lower.

Thus, the method used has been proven to be robust when initial corrections to the spacecraft position were required, asserting its validity for every descent maneuver made when both the initial and final position points are enclosed within the range of points defined in the acceleration mesh.

4.4 Landing on Stickney crater

As described in the introduction to this Thesis, a considerable number of scientific studies about Phobos have been made in the last three decades concerning the origin of this satellite, as well as a characterization of a model mission that could clarify the lack of knowledge present nowadays about it. Detailed descriptions can be found in [32] and [2], where a thorough analysis of the scientifically-interesting landing sites is made. In Figure 1.2 of this Thesis, the main ones can be observed, with the most important ones listed below. Although the preferred landing site would depend on the type of mission carried out, there is one crater that stands among the others, the Stickney crater. This is mainly because it is the largest crater on Phobos' surface, with its interior walls presenting a lineated texture, due to the landslides of regolith present on the boundaries of the crater that fall inside of it [33]. Therefore, the Phobos landing analysis made in this Thesis would not be complete without having studied a landing maneuver to the Stickney crater.

Firstly, to make a more clear visualization of the Stickney Crater characteristics, the following image taken by the Mars Reconnaissance Orbiter (MRO) mission is attached

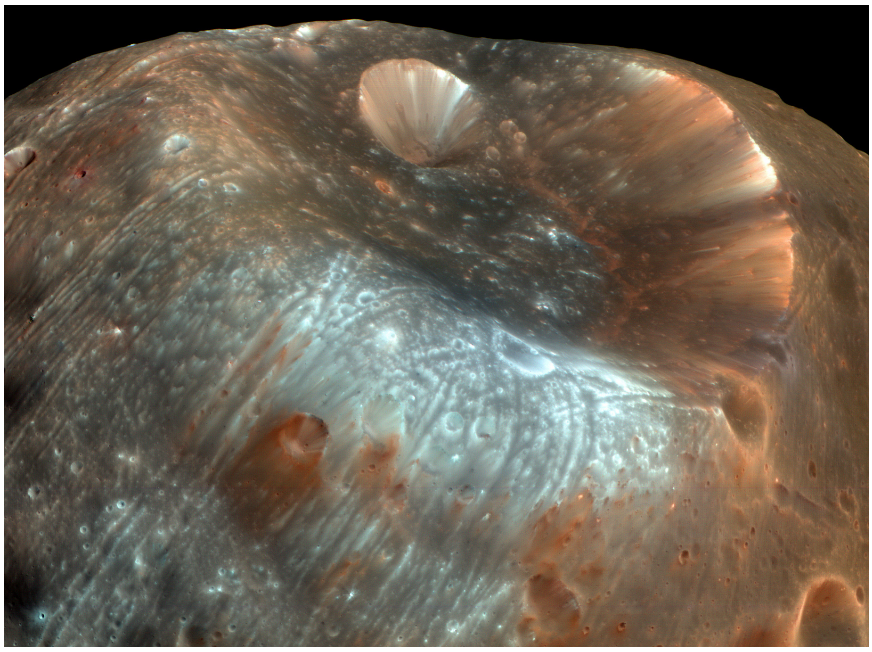

Figure 4.12: Stickney crater. Image taken by the MRO

In order to perform the landing maneuver, its location on Phobos' surface must be known. According to [34], its location is 1^0N 49^0W. Thus, obtaining the Cartesian coordinates associated to the location given is straightforward, by knowing that

$$r\,sin\phi = z \tag{4.26}$$

$$r\,cos\phi = \sqrt{x^2 + y^2} \tag{4.27}$$

$$tan\theta = \frac{y}{x} \tag{4.28}$$

where θ is the azimuth angle and ϕ is the elevation angle. Hence, expressing the location as a proportion of the radius in Cartesian coordinates results in

$$x = 0.656R \tag{4.29}$$

$$y = -0.75R \tag{4.30}$$

$$z = 0.0175R \tag{4.31}$$

The problem that is going to be solved is a descent towards Phobos' surface from an initial point located 20 meters further from the coordinates specified in (4.29), (4.30) and (4.31), thus implying a descent along a straight line. The results of using the same mesh as in previous cases did not give an optimal solution, but a

quasi-optimal one. This occurred mainly because the Stickney crater is defined by coordinates that need a much bigger mesh definition than the previous one, as aforementioned, since a much larger portion of space must be included into the mesh calculated. Because of that, the acceleration error when analyzing this case was higher, which implied that the mesh had to be re-defined in order to include all the Phobos volume. Note that the Stickney crater is the most scientifically-interesting landing site and, at the same time, the most difficult one to deal with when implementing the interpolation method, making it a perfect situation to evaluate whether re-defining the mesh can make the problem converge to a completely optimal solution.

The relative error analysis was computed again for this extended mesh, resulting in $N = 20$ number of points required for the error to be smaller than $\mathcal{O} \sim 10^{-2}$. This enhanced number of points derived in a much larger computational time required for obtaining the acceleration grid; in fact, the ratio between $N = 20$ and $N = 9$ resulted in

$$Ratio \equiv \frac{3 \times 20^3}{3 \times 9^3} \approx 11 \tag{4.32}$$

Therefore, the computational time required for this second acceleration grid was eleven times higher than the previous one.

By using this extended mesh, the optimality conditions were fulfilled for this case, with the following results obtained

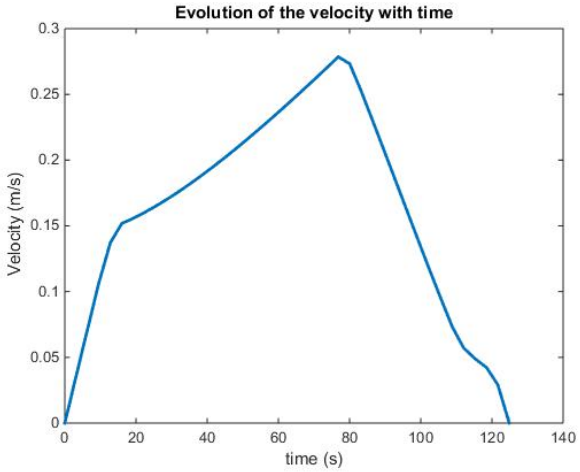

Figure 4.13: Variation of the velocity magnitude with time.

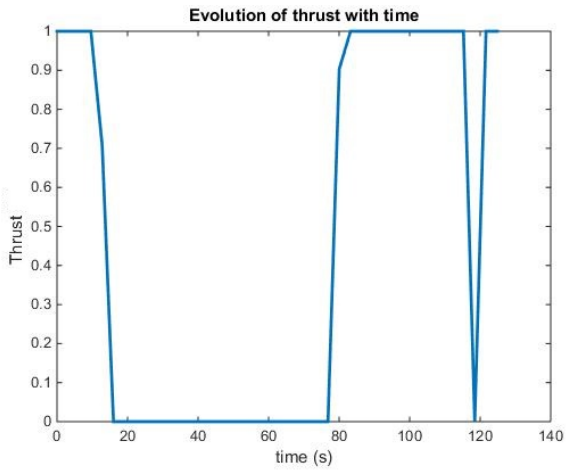

Figure 4.14: Variation of the thrust magnitude with time

In this case, the landing maneuver is started when hovering around Phobos; hence, the initial velocity for the three components is equal to zero. As can be observed in the

previous image, the spacecraft velocity will increase due to the attraction that Phobos exerts on it. At a time close to 80 seconds, the thrust is turned on, thus reducing the velocity. Note that an irregularity is present at 110 seconds, which is mainly due to the convexity of the crater studied, which will result in a more complicated acceleration evolution as compared to the first case analyzed in the previous section. Finally, the velocity goes to zero, thus assuring that an optimal solution has been found.

Therefore, both the extended mesh and the one created for the first and second analyses are available and robust enough for solving a landing trajectory to Phobos. The extended one allows to select any position on Phobos surface, at the cost of producing a larger error in the computations, while the first one should be used when a descent maneuver close enough to the surface (less than 50 meters) is made.

As a concluding remark, it must be pointed out that the acceleration computation would produce no error (apart from the intrinsic one that the Polyhedron method possesses, like any other method), if there were sufficiently large computational resources available, since the Polyhedron method could be directly implemented in this case. As stated before, the code is prepared in case of having more powerful computers, so any trajectory could be tested in that case. While not having them, the interpolation method has been proven to be robust enough, with either the extended or the basic mesh chosen depending on the height from which the landing maneuver is started, and the location at which the spacecraft should touch Phobos' surface.

Chapter 5

Conclusions and Future Work

5.1 Results review and final discussion

A landing maneuver treated as a Low-Thrust Optimal Control Problem has been solved in this Thesis. The solution of this Optimal Control Problem, characterized by the dynamical constraints (3.2), (3.3), (3.4) and the path constraint (3.22), has been obtained by using the Collocation method included in GPOPS.

Moreover, a very precise acceleration computation method has been implemented, by which the exact value of the acceleration is introduced into the dynamical equations at each of the points for which the spacecraft trajectory is discretized. Unfortunately, the Polyhedron method elaborated in [16] and modified in the coding work developed in this Thesis could not be directly implemented into the Optimal Control Problem, in order to obtain the exact value of the acceleration at each trajectory node; computational resources were limited in this case, as aforementioned.

It was therefore necessary to develop an interpolating method, by which the acceleration value at a given node could be obtained by knowing the exact acceleration value at neighboring points, with the acceleration value at those points computed beforehand with the Polyhedron method code and implemented into the defined mesh. As studied in Chapter 4, the amount of error that this interpolating method introduced into the computation was minimal, once a given number of points was exceeded (in the case analyzed, a number of points N = 9 was sufficient in order to obtain an error $\mathcal{O} \sim 10^{-4}$). Three different cases were tested, differing in the fact that the initial position for the first and third cases was placed in the radial direction, whereas for the second one it was not. An optimal solution was found in the three cases, which assures the robustness of the method used.

In the third case, however, a much larger mesh volume was required, which implied redefining this mesh with a sufficient number of points such that the relative error

in the acceleration error was small. Both meshes have proven to be robust, and the election of one of them should be made based on the location of the landing point targeted.

In case a larger amount of computational resources are available, the Polyhedron method code could directly obtain the acceleration for each of the nodes for which the spacecraft trajectory is discretized, thus obtaining an Optimal Control Problem solution with the exact value of the gravity acceleration parameter at each point of the spacecraft trajectory. The codes are already adapted to account for this fact; hence, the implementation and the obtainment of results would be direct.

It must be noted, nonetheless, that the error committed by using the Polyhedron method is smaller (as stated in Chapter 4), than the uncertainty that the density parameter introduces into the analysis, with this parameter defined in Chapter 3. Therefore, a more accurate quantification of the density would result in a larger decrease in the global uncertainty than the change in the acceleration computation method.

Since a Martian system mission is a field of research in Astronautics nowadays, it would be logical to continue the trend followed in this Thesis by implementing other perturbations that can affect the spacecraft dynamics, as explained in the next section.

5.2 Limitations of the results

The main limitation in this study is the consideration that the spacecraft dynamics are accurately described by treating the landing maneuver as a 2 Body Problem (2 BP), without considering Mars a perturbation; in fact, Phobos is placed inside the Martian gravitational field [6], and it is still under investigation whether it is also located inside its magnetosphere [8]. Although this hypothesis is valid for a general study, it will not be sufficiently accurate when a mission to Phobos has to be accurately described. In addition to the Martian influence, other perturbations should be also introduced, such as the influence that the Sun (quantified by the solar wind [8]) or Deimos (by the gravitational attraction force that this Martian moon causes on Phobos [6]) produce. This would greatly enhance the difficulty of giving a result for the dynamics problem; in fact, no article has been found in which the perturbations due to bodies other than Mars, Deimos and the Sun have been implemented in a Phobos' study. Implementing these influences as perturbations would be in fact another source of inaccuracy; hence,

a N-body problem (NBP) should be considered, in which deterministic chaos and non-planar motion would play a role. Note that, in that case, the equation of motion for each of the N-bodies should be

$$m_i \ddot{r}_i \equiv F_i = \sum_{j \neq i} G \frac{m_i m_j}{r_{ij}^3} r_{ij} \tag{5.1}$$

for i = 1, ..., N.

Another limitation of this study is the fact that the results obtained are based on the actual Phobos data available from [26], in which a considerable uncertainty in the density parameter (around a 1%) is included. It must be noted, nonetheless, that Phobos' shape and gravity are not sufficiently known nowadays, with the shape estimation having a 2% uncertainty in global volume according to [35]. Therefore, a much more precise analysis could be made by using new techniques to determine the shape and volume of Phobos. According to [6], either laser ranging or stereo photoclinometry techniques would provide more accurate data, having been previously used in order to measure the shape of asteroids Eros and Itokawa, and Itokawa and Vesta respectively.

Moreover, there is some phenomena that is not completely modeled up to this day and that may result in an important change in the spacecraft dynamics; these are, according to [2]

- The synchronous orbit that Phobos has with Mars.
- The tidal accelerations across Phobos.
- The centrifugal accelerations due to the short Phobos rotation rate.

As a 2 BP is being analyzed, neither the Circular Restricted Three-Body Problem (CR3BP) nor the Clohessy-Wiltshire (CW) equations are used; they could not be used anyway, since these equations need to be applied on a circular orbit problem in order to obtain accurate results; Phobos has, unfortunately, a non-perfectly circular orbit [5].

Other perturbations should be also included into the dynamical constraints of the problem, such as the thermal, solar and albedo forces; however, as they depend on the imperfect Phobos shape and the reflectivity models, they would also become another source of uncertainty [5].

5.3 Roadmap for future work

Firstly, the perturbations due to Mars and Deimos should be modeled and implemented into the analysis. According to [36], the former are mainly due to the Mars' gravitational field and its oblateness, while the latter are caused by the mutual attraction that both satellites experiment. Moreover, the perturbation produced by the thermal, solar and albedo radiation pressures should be also implemented into the dynamical constraints. In a further analysis, perturbations due to other planets should be modeled too, because of the attraction force that Phobos could experiment due to them; all these considerations would increase remarkably the accuracy of the analysis, although additional uncertainty, intrinsic to these implemented models, would also enter into the computation. Besides, as previously stated, an increase in the Phobos' shape data accuracy could imply a reduction in uncertainty of around a 2%.

Further improvements could be obtained by changing the method by which the spacecraft position is known. In particular, optimal navigation implementation would allow to know in better detail the body-relative states [5], although this approach should be taken as a parallel study to the one developed; it would mainly cover the Navigation part of the *Guidance, Navigation and Control* (GNC) problem. Extensive studies have been developed in this field up to date, with [37] being one of the most detailed ones. It consists in parametrizing the relative dynamics through relative orbital elements, a method which allows implementing a detailed dynamical model, with effects such as Phobos' oblateness being covered.

Another interesting approach is the development of non-linear methodologies used to implement real-time algorithms suitable for guidance and control of the spacecraft during close-proximity operations [38], which would then close the study of the GNC problem. The guidance laws required to generate autonomous thrust commands depending on the spacecraft state are developed based on a combination of optimal and Sliding Control theory. Moreover, by using Lyapunov second theorem, the non-linear guidance laws are proven to be stable against perturbations with known upper bound.

An improvement of the previous theory is described in [39], in which a guidance law which is stable and robust against bounded unknown perturbations is developed. In this case, the *Multiple Sliding Surface Guidance* (MSSG) algorithm can generate an acceleration command by knowing just the current and the final target state, thus not requiring any off-line trajectory generation.

There are, nonetheless, further improvements required in [39], among others, in order to increase the algorithm's robustness in more strenuous conditions

- Inclusion of additional constraints in the algorithm's development process, such as glide-slope constraints and attitude/thrust constraints.
- A continuous update process of the set of the optimal set of guidance parameters, which will reinforce the algorithm during the descent phase.
- Implementation of the new algorithm features into different scenarios, such as a terminal powered landing guidance.

Hence, it can be clearly appreciated that there is a huge field of improvement in this area, with the accuracy of the analysis increasing with the large amount of computer resources improvements expected in future years.

Appendix A

Socio-Economic context

The fall of the Berlin Wall in 1989, with the subsequent USSR's disappearance, marked the end of the Cold War and, with it, the end of the space race between the soviets and the americans. This directly derived in a reduction of the percentage of the United States GPD invested in NASA, from around a 1% in 1990 to almost 0.5% in the 2010s. Please refer to *The World Almanac and Book of Facts* in order to find the exact numbers from NASA's foundation until 2016 (note that no citation is made, since the book is updated each year since 1868, with a detailed description of NASA's budget since its creation in 1958). During the past decades, private companies have emerged in this space manufacturing sector, such as Virgin Galactic or Space X.

Since the Cold War period, there has been scientific interest in exploring the Martian system. The first mission to examine Phobos was laid off and operated by the USSR, consisting in launching the Phobos 1 and Phobos 2 spacecraft. According to [14], the mission scientific aim was to explore Mars and Phobos. Both spacecrafts were equipped with an autonomous systems controlled by signals transmitted from the Earth. After the commands were sent to the probe, the onboard computers would handle them, executing a predetermined function of the scientific instruments. The result of the samples' analysis would be transmitted back to a signal station in the Earth. Two different space probes were launched: Phobos 1, and Phobos 2. Unfortunately, both missions failed to achieve their objectives [40].

Four different missions have been proposed in recent years [6], with only the Phobos-GRUNT spacecraft becoming a reality

- **Phobos-GRUNT**. This mission was developed by the *Russian Space Agency*, with a survey satellite built by the *China National Space Administration*. It consisted in landing the spacecraft on Phobos, collecting regolith by means of

a robotic arm and returning the samples in a small capsule. Unfortunately, the spacecraft could not make the subsequent burns necessary to leave the Earth's orbit for heading towards Mars, reentering into the Earth's atmosphere in January 2012.

- **Gulliver**. The mission plan called for returning a sample from Deimos, and a touch-and-go technique would have been used to collect a kilogram-sized sample of regolith with minimum spacecraft-surface interaction.

- **Aladdin**. This mission was primarily characterized for taking samples of both Phobos and Deimos surfaces without landing on either of them. Instead, the spacecraft would launch a cluster of projectiles to impact the moon's surface, fly through the debris, and collect samples on a carpet-like pad. A capsule with the samples would then return to the Earth, in order to analyze them at the Utah Test and Training Range (UTTR).

- **Merlin**. It was a mission planned in order to determine the elemental and mineralogical composition of one of Mars' moons, as well as its volatile and organic content, and characterize the surface and processes that have modified it. The spacecraft would effectively land on one of the martian moon's surface, a maneuver which would last for 90 days. Please refer to [41] in order to read the study that set up this mission, with a thorough explanation of the different technical aspects involved.

- **Hall**. It is planned to be a New Frontiers-class mission, in which solar electric propulsion will be used to rendezvous with and sample both Phobos and Deimos. The mission plan will consist in landing and sampling Phobos on, at least, two different locations; then, a landing operation on Deimos' surface will be carried out, extracting samples at one location. The capsule, with 1 Kg of regolith inside, would then return to the Earth, and land on the UTTR. The complete mission description can be found in [15].

In addition to the previously described missions, private companies have announced their interest in successfully completing a spacecraft landing in Mars in the next decade; in fact, Space X claims [42] that one of their capsules will land on Mars' surface in 2018, for the sake of sending humans in 2024.

From the most logical and rigorous scientific point of view [7], the optimum mission opportunity to launch an spacecraft to the Martial system will occur in 2033 and 2035, due to two main reasons:

- The round trip delta V from the Earth to Mars will be at the lowest point in those two years, since, because of the Martian orbit eccentricity, this parameter varies over a 15 year cycle; this would also result in a lower Earth reentry velocity required.

- The Sun's magnetic field will be in its most active phase of its 11 year cycle, which would reduce the flux of cosmic rays entering the inner solar system. This would in turn reduce the astronauts radiation risk.

Finally, it must be mentioned that the *Japan Aerospace Exploration Agency* (JAXA) is also exploring the possibility of sending a spacecraft to Phobos or Deimos, with the purpose of collecting regolith samples [43], which could occur as soon as 2022.

Hence, there are political, economical and scientific aspects hidden behind the exploration of the Martian system; depending on which of them weights more, the missions will occur before (in the 2020s) or after (in the 2030s, if an strictly scientific approach is taken).

Appendix B

Budget

It is very ventured at this point of the analysis to establish a cost for the complete mission, as it would depend on the exact type of scientific objectives that are aimed to be accomplished, the actual budget constraints of the manufacturing company and the level of accuracy in the results that the mission requires (which would then result in, whether there is an In-situ analysis of the samples taken or a capsule is returned to the Earth for the regolith to be analyzed).

There are, nonetheless, several missions that have been operated (some of them being still active), at other destinations with similar scientific objectives; hence, the total cost of these missions could be considered, in a first approximation, as a reference for the Phobos mission designed.

- **Rosetta mission**. The total cost of the Rosetta mission is, according to [44] close to 1.4 billion Euros, with 220 million Euros being covered by the lander (Philae); note that, in the analysis made in this Thesis, only the lander characteristics have been implemented into the analysis, since a descent maneuver close to the Phobos surface has been considered. Hence, the lander cost would give the specific budget of the mission (the cost for this part of the mission), taking into account that the total cost will be accounted for when analyzing the feasibility of the complete mission. The mission cost covers development and construction of the spacecraft and all of its instruments, including the lander, together with launch and operations.

- **Phobos 1**. This spacecraft, together with Phobos 2, are the two only probes that have been ever sent to Phobos, although both missions failed before reaching the Martian moon's surface. The cost of this mission was about 300 million dollars [14].

- **OSIRIS-REx**. According to [45], the OSIRIS-REx spacecraft will travel to Bennu, a near-Earth asteroid, bringing at least a 60-grams sample back to Earth for study, with the objective of investigating the composition of the very early solar system and the source of organic materials and water that made their way to the Earth. The lander's total cost will go up to 183.5 million dollars [46], with a total estimated mission cost of around 800 million dollars.

- **Beagle 2**. The objective of this Martian mission was to characterize the geology, mineralogy, geochemistry and oxidation state, the physical properties of the atmosphere and surface layers, collect data on martian meteorology and climatology, and search for signatures of life in the Martian surface [47]. Although an exact cost of the mission has not been documented, an estimation could be made, according to [48], around $65 million-$80 million. This mission, although centered on Mars, can give a general idea of both the lander characteristics and its cost.

As aforementioned, an exact cost for the mission considered cannot be provided, since its scientific objectives have to be completely defined first, as well as the robotic instruments carried on-board. Note that the fluctuations in the currency, and the country from which the space agency originates, will also play a major role, as these two factors will define the currency with which the budget will be made, with the strength of the currency determining whether it should be more advisable for the mission to be manufactured in another economic region. However, a cost estimation can be made from the scientifically-similar described missions, with a rough estimate in the range of $400 million-$800 million.

The budget required to develop this Thesis in a professional way can be also calculated. The different costs can be classified as follows:

- **MATLAB Commercial License R2016b**. This purchase

  - Offers choice between two activation types: Standalone Named User and Designated Computer.
  - Allows installation on the following platforms: Windows, Linux, and Macintosh.

  The previous description is taken from [49], in which the cost of the license is also fixed in 2000 €.

- **Aerospace Engineer salary**. The salary of the aerospace engineer developing this work must be also accounted for. The contract shall run for four months, the time required for this Thesis to be finalized. According to [50], the average annual salary for an aerospace engineer in Spain is 29423 €, thereby resulting in a monthly salary equal to 2452 €. Note that the gross salary is regarded here; the Social Security cost is not included in this balance sheet, since the year at which the project will become a reality is not fixed, and the Spanish Government updates annually the quotation cost dedicated to the Social Security, depending on the professional category held. Please refer to [51] in order to find the contribution bases for the present year.

- **Studio Rent**. Finally, the rent that is paid for the studio must be also considered. According to [52], it will cost about 3000 € per month.

The costs analyzed are summarized next, together with the total cost of the project.

	Cost per month (€)	Total Cost per item (€)
MATLAB Commercial License	-	2000
Engineer Salary	2452	9808
Studio Rent	3000	12000
Total Cost	5452	**23808**

Table B.1: Project Cost Summary

Hence, in this annex both the project cost and the budget for a real mission to Phobos have been accurately described, in order to close the analysis made in this Thesis.

Bibliography

[1] H. Yang and H. Baoyin. Fuel-optimal control for soft landing on an irregular asteroid. *IEEE Trans. Aerospace and Electronic Systems*, 51(3):1688–1697, 2015.

[2] A. F. Abercromby, S. Chappell, D. Lee, A. Howe, and M. Gernhardt. Human Exploration of Phobos. *Proceedings of the IEEE Aerospace Conference, Big Sky, MT*, 2015.

[3] R. A. Werner and D.J. Scheeres. Exterior Gravitation of a Polyhedron Derived and Compared with Harmonic and Mascon Gravitation Representations of Asteroid 4769 castalia. *Celestial Mechanics and Dynamical Astronomy*, 65:313–344, 1997.

[4] C. R. Hargraves and S. W. Paris. Direct trajectory optimization using nonlinear programming and collocation. *Journal of Guidance, Control, and Dynamics*, 10(4):338–342, 1987.

[5] M. S. Wallace, J. S. Parker, N. J. Strange, and D. Grebow. Orbital Operations for Phobos and Deimos Exploration. *AIAA/AAS Astrodynamics Specialist Conference*, 2012.

[6] S.L. Murchie, D.T. Britt, and C.M Pieters. The value of Phobos Sample Return. *Planet. Space Sci*, 102:176–182, 2014.

[7] W. Pratt and J. Hopkins. Comparison of Deimos and Phobos as destinations for human exploration and identification of preferred landing sites. *AIAA SPACE 2011 Conference & Exposition*, 2011.

[8] I.S. Veselovsky. Is Phobos Magnetized? *Astronomicheskii Vestnik*, 38(3):218–224, 2004.

[9] W. Hartmann. Additional evidence about an early intense flux of asteroids and the origin of Phobos. *Icarus*, 87:236, 1990.

[10] D. Hunten. Capture of Phobos and Deimos by protoatmospheric drag. *Icarus*, 37:113, 1979.

[11] V.S. Safronov, G.V. Pechernikova, E.L. Ruskol, and A.V. Vitjazev. Protosatellite swarms. *In: Burns, J., Matthews, M., University of Arizona*, 102:89, 1986.

[12] M. Carr et al. Humans to the Martian system: Summary of strategic knowledge gaps. *Report of the MEPAG Precursor Science Analysis Group*, 2012.

[13] B. Drake. Human exploration of Mars design reference architecture 5.0. *NASA/SP*, 566, 2009.

[14] Y. B. Zeldovich, A. A. Ruzmaikin, and D. D. Sokolof. *The Almighty Chance*. World Scientific, Singapore, 1990.

[15] P. Lee et al. Hall: a Phobos and Deimos sample return mission. *Lunar Planet*, 41 (Abstract 1633), 2010.

[16] Diego García Pardo. Analysis and implementation of gravity field models for planets and asteroids. Bachelor thesis, Universidad Carlos III de Madrid, June 2014.

[17] E Thomas, J. Veverka, and S Dermott. 17 Small Satellites. *Satellites, J.A. Burns and M.S. Matthews (eds.), Tucson: University of Arizona Press*, pages 802–835, 1986.

[18] W.D. MacMillan. *Dynamics of Rigid Bodies*. McGraw-Hill, New York, 1936.

[19] P. Geissler, J.-M. Petit, D. Durda, R. Greenberg, W. Bottke, M. Nolan, and J. Moore. *Icarus*, 120:140, 1996.

[20] W.M. Kaula. *Theory of Satellite Geodesy*. Blaisdell, Waltham, 1966.

[21] Anil V. Rao, David A. Benson, Christopher Darby, Michael A. Patterson, Camila Francolin, Ilyssa Sanders, and Geoffrey T. Huntington. Algorithm 902: GPOPS, a MATLAB software for solving multiple-phase optimal control problems using the Gauss Pseudospectral Method. *ACM Transactions on Mathematical Software (TOMS)*, 37(2):1–39, 2010.

[22] David Morante González. A comparative study of optimal control algorithms using ideal frame references. Bachelor thesis, Universidad Politécnica de Madrid, November 2014.

[23] Andreas Wachter Stefan Vigerske. *Introduction to Ipopt: A tutorial for downloading, installing and using Ipopt.* Technical report, Carnegie Mellon University, 2014.

[24] Taylor and Francis. *Applied Optimal Control: Optimization, Estimation and Control*. 1975.

[25] B.A. Conway. *Spacecraft trajectory optimization*. Cambridge University Press, 2010.

[26] T. P. Andert, P. Rosenblatt, M. Ptzold, B. Husler, V. Dehant, G. L. Tyler, and J. C. Marty. Precise mass determination and the nature of Phobos. *Geophysical Research Letters*, 37:L09202, 2010.

[27] Y.F. Kolyuka, A.E. Efimov, S.M. Kudryatsev, O.K. Margorin, V.P. Tarasov, and V.F Tikhonov. Refinement of the gravitational constant of Phobos from PHOBOS-2 tracking data. *Soviet Astronomy Letters*, 16(2):168–170, 1990.

[28] I. Katz D.M. Goebel. *Fundamentals of Electric Propulsion: Ion and Hall Thrusters*. Wiley, New Jersey, 2008.

[29] J. M. Sankovic, J. A. Hamley, and Thomas W. Hang. Performance Evaluation of the Russian spt-100 Thruster at NASA LeRC. *Proceedings of the 23rd International Electric Propulsion Conference, IEPC-93-094*, 1993.

[30] ESA. Ion engine gets SMART-1 to the Moon: Electric Propulsion Subsystem, August 2006. `http://www.esa.int/Our_Activities/Space_Science/SMART-1/Ion_engine_gets_SMART-1_to_the_Moon`.

[31] R.W. Gaskell. Gaskell phobos shape model v1.0. vo1-sa-visa/visb-5-phobosshape-v1.0. *NASA Planetary Data System*, 2011.

[32] A. F. Abercromby, S.P. Chappell, A. Howe, M. Gernhardt, O.S. Bekdash, E.Z. Crues, K.H. Beaton, Z.Q. Lin, and P. Bielski. Human and Robotic exploration missions to Phobos prior to crewed Mars surface missions. *IEEE Aerospace Conference, Big Sky, MT*, 2016.

[33] John B. Murray et al. New evidence on the origin of Phobos' parallel grooves from HRSC mars express. *Lunar and Planetary Science*, XXXVII, 2006.

[34] Jennifer Blue. Stickney. USGS astrogeology research program. *Gazetteer of Planetary Nomenclature*.

[35] R.A. Jacobson. The Orbits and Masses of the Martian Satellites and the Libration of Phobos. *The Astronomical Journal*, 139(2):668–679, 2010.

[36] R. A. Jacobson and V Lainey. Martian satellite orbits and ephemerides. *Planetary and Space Science*, 102(2):35–44, 2014.

[37] S. *D'Amico*, G. Gaias, and J. S. Ardaens. Angles-only navigation to a noncooperative satellite using relative orbit elements. *Journal of Guidance, Control, and Dynamics*, 37(2), 2014.

[38] R. Furfaro, B. Gaudet, D.R. Wibben, and J. Simo. Development of non-linear guidance algorithms for asteroids close-proximity operations. *AIAA Guidance, Navigation, and Control (GNC) Conference*, 2013.

[39] R. Furfaro, B. Gaudet, D.R. Wibben, and J. Simo. Terminal multiple surface sliding guidance for planetary landing: development, tuning and optimization via reinforcement learning. *Journal of Astronaut Science*, 62:73–99, 2015.

[40] R. Z. Sagdeev and A. V Zakharov. Brief History of the Phobos Mission. *Nature*, 341:585, 1989.

[41] S. Murchie, D. Eng, N. Chabot, Y. Guo, R. Arvidson, A. Trebi-Ollennu, F. Seelos, E. Adams, and G. Fountain. MERLIN: MarsMoon exploration, reconnaissance and landed investigation. *Acta Astronaut*, 2012.

[42] Kenneth Chang. SpaceX Says It Plans to Send a Probe to Mars, April 2016. `http://www.nytimes.com/2016/04/28/science/mars-spacex-dragon-landing-2018.html?_r=0`.

[43] Devin Coldewey. Japan Plans Rock-Collecting Trip to Martian Moon Phobos or Deimos, June 2015. `http://www.nbcnews.com/science/space/japan-plans-rock-collecting-trip-martian-moon-phobos-or-deimos-n374701`.

[44] ESA. Rosetta's Frequency Asked Questions. `http://www.esa.int/Our_Activities/Space_Science/Rosetta/Frequently_asked_questions`.

[45] NASAs OSIRIS-REx Mission Passes Critical Milestone, March 2015. `http://www.nasa.gov/press/2015/march/nasa-s-osiris-rex-mission-passes-critical-milestone`.

[46] Soderman. NASA Selects Launch Services Contract for OSIRIS-REx Mission. http://sservi.nasa.gov/articles/nasa-selects-launch-services-contract-for-osiris-rex-mission/.

[47] I. P. Wright et al. Scientific objectives of the Beagle 2 lander. *Acta Astronaut*, 52:219–225, 2003.

[48] David R. Williams. Beagle 2. http://nssdc.gsfc.nasa.gov/nmc/spacecraftDisplay.do?id=2003-022C.

[49] Pricing and Licensing of the MATLAB program. http://es.mathworks.com/pricing-licensing/index.html?intendeduse=edu&prodcode=ML.

[50] Aerospace Engineer salary. http://www.payscale.com/research/ES/Job=Aerospace_Engineer/Salary.

[51] Social Security. http://www.seg-social.es/Internet_1/Trabajadores/CotizacionRecaudaci10777/Regimenes/RegimenGeneraldelaS10957/InformacionGeneral/index.htm.

[52] Studio Rent. http://www.idealista.com/inmueble/33757335/.